LiU-ITN-TEK-A--10/064--SE

Thermal Conductivity Measurement of PEDOT:PSS by 3-omega Technique

Farshad Faghani

2010-10-21

Linköpings universitet
TEKNISKA HÖGSKOLAN

Department of Science and Technology
Linköping University
SE-601 74 Norrköping, Sweden

Institutionen för teknik och naturvetenskap
Linköpings Universitet
601 74 Norrköping

LiU-ITN-TEK-A--10/064--SE

Thermal Conductivity Measurement of PEDOT:PSS by 3-omega Technique

Examensarbete utfört i elektroteknik
vid Tekniska Högskolan vid
Linköpings universitet

Farshad Faghani

Handledare Xavier Crispin
Examinator Xavier Crispin

Norrköping 2010-10-21

ABSTRACT

Conducting polymers (CP) have received great attention in both academic and industrial areas in recent years. They exhibit unique characteristics (electrical conductivity, solution processability, light weight and flexibility) which make them promising candidates for being used in many electronic applications. Recently, there is a renewed interest to consider those materials for thermoelectric generators that is for energy harvesting purposes. Therefore, it is of great importance to have in depth understanding of their thermal and electrical characteristics. In this diploma work, the thermal conductivity of PEDOT:PSS is investigated by applying 3-omega technique which is accounted for a transient method of measuring thermal conductivity and specific heat.

To validate the measurement setup, two benchmark substrates with known properties are explored and the results for thermal conductivity are nicely in agreement with their actual values with a reasonable error percentage. All measurements are carried out inside a Cryogenic probe station with vacuum condition. Then a bulk scale of PEDOT:PSS with sufficient thickness is made and investigated. Although, it is a great challenge to make a thick layer of this polymer since it needs to be both solid state and has as smooth surface as possible for further gold deposition.

The results display a thermal conductivity range between 0.20 and 0.25 ($W.m^{-1}.K^{-1}$) at room temperature which is a nice approximation of what has been reported so far. The discrepancy is mainly due to some uncertainty about the exact value of temperature coefficient of resistance (TCR) of the heater and also heat losses especially in case of heaters with larger surface area. Moreover, thermal conductivity of PEDOT:PSS is studied over a wide temperature band ranging from 223 - 373 K.

PREFACE

This diploma work was carried out in the Organic electronic group at Science and Technology Department (ITN) of Linköping University (LIU) during March to August 2010. The material for this work was mainly collected from previously published papers and some reference books in this field of research. Also the whole measurement processes were performed in clean room co-owned between ACREO AB and LIU located in Norrköping, Sweden.

My deepest appreciation belongs to my examiner, Professor Xavier Crispin for his helpful comments along the project. Also, I should thank you for your trustfulness to give me the opportunity of taking such a fascinating subject in my diploma work. It brought me valuable experiences of working in clean room and to be practically familiar with various measuring and fabrication techniques. Thank you for believing in me!

I should also specially thank my supervisor, Zia Ullah Khan, for his inexhaustible efforts in assisting me with all steps of this work from introducing the experimental set up to sample preparation and method implementation. I really appreciate you for everything!

I would also like to express my gratitude to all OrgEl group members for their nice and warm attitude towards me during the time which I spent there. I'll never forget you all!
Meanwhile, it is my great pleasure to thank Mahziar Namedanian, Sara M. Razavi, Arash Matinrad and Negar A. Sany for their comprehensive supports during this work. I really owe you my dear friends!

But above all, I would like to send my ultimate love to my parents for their permanent support during whole my life. I LOVE YOU!!

Norrköping 8.8.2010

Farshad Faghani

Table of Contents

LIST OF FIGURES

LIST OF TABLES

CHAPTER 1

1. INTRODUCTION

Nowadays, the fundamental limit of non renewable resources of energy and the environmental issues lead our society to pay more attention on energy consumption and saving measures. In average the various energy sources (e.g. fossil, nuclear, solar radiation,…) can be transformed into electricity with a rather low efficiency of 35%; that is 65% of the energy source is lost in waste heat. 50% of the waste heat is stored in large volume of warm fluids (T<200°C) for which there is no viable technology for energy transducers. Thermoelectric generators account for innovative apparatus, more especially energy transducers, to transform waste heat and natural heat source directly into electricity. To extract the energy from large volume of fluids, one would need to functionalize the large area of heat exchangers with thermogenerators. However, the actual thermoelectric materials and the process of fabrication of thermogenerators are too expensive to make this a solution.

Organic semiconductors and conducting polymers are low cost materials that can be processed from solution, thus making available low-cost manufacturing techniques such as printing. Those materials are potentially interesting for thermoelectric applications and their thermal properties (conductivity, diffusivity) have been little suited up to now. By increasing the application of new generation of materials with sophisticated structure, it is of great importance to have in depth understanding of their thermal and electrical characteristics. Semiconductors and especially organic ones have some unique characteristics which make them promising candidates for thermoelectric applications.

1.1. GOAL OF THE THESIS

The focus for this diploma work is an investigation into thermal conductivity of the conducting polymer called PEDOT:PSS. This conducting polymer is thought to be an ideal candidate for converting waste heat to electrical energy. Although the current thermoelectric characteristics, especially electrical conductivity, is not comparable to inorganic ones but many research and study has been conducted within recent years to fill the existing gap.

Thermal conductivity is one of the most important physical properties of each substance which need to be investigated. In this regards, the necessity for improvement of conventional measurement methods has emerged.

1.2. METHODOLOGY

There are different methods for measuring thermal conductivity. They can be categorized in two branches; steady state and transient techniques.

In this diploma work, we opt for 3ω measurement method which is classified in transient techniques. In order to catch the above mentioned goal, at first step, the accuracy of the implemented 3ω measurement set up is validated by two known reference specimens with different ranges of thermal conductivity. Then, it is required to make a thick layer of PEDOT:PSS prior to making any measurement.

Some examples of each technique are briefly discussed in below.

1.2.1. STEADY STATE METHOD

This technique is usually employed for measuring thermo-physical behavior of medium to large size specimens and requires long time to reach thermal equilibrium. Below is a brief explanation of Guarded Hot Plate method (GHP) as an example.

- **Guarded Hot Plate method (GHP)**

This primary method is mainly used for determination of the thermal performance of large scale insulations and other materials of high thermal resistance. This method is capable of measuring thermal conductivity in a range between 0.01 and 6 ($W.m^{-1}.K^{-1}$).

The earliest prominent publication using this technique was reported in the year 1916 when Dickinson and Van Dusen investigated about heat flow through air space and 30 insulating materials [1].

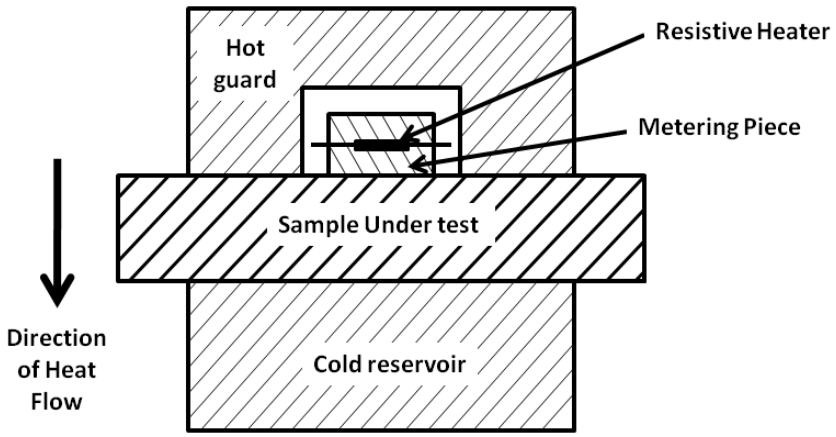

FIGURE 1-1: SKETCH OF THE GUARDED HOT PLATE APPARATUS [2]

The procedure is placing the specimen of interest between two different flat plates surrounded by guard heater (figure 1-1). Heat is produced in one plate by an inner electric heater and passes through the specimen and sunk by the cold plate. The guarded heater provides as straight heat

conduction as possible through the specimen by maintaining the peripheral temperature of the specimen at constant level. As a result, any deflection in heat conduction path from hot to cold plate is hindered. After the specimen reaches to thermal equilibrium, its average thermal conductivity, k, can be obtained as follows:

$$k = \frac{P.d}{A.dT} \qquad 1\text{-}1$$

Where P is the electrical power input to the main heater, A is the main heater surface area, dT is the temperature difference between two plates, and d indicates the specimen thickness.

1.2.2. TRANSIENT METHOD

Transient method comprises a large group of techniques which serve for measuring thermal conductivity of materials. Employing this technique has been increasingly popular in the past three decades and is continuously evolving with new improvements. They are much faster than traditional ones and suit also small scale specimens.

The general geometry for this technique is using either a plane or a wire/strip heat source which simultaneously can be used as thermometer. This source heater is dominantly sandwiched between two identical pieces of specimen. It is stimulated by a favorable input signal current and resulting heat is propagated in the specimen. Then by monitoring the temperature change during the measurement time, one can derive the value of thermal conductivity for the specimen [3]. However, in case of 3ω technique, there are some differences which will be mentioned later in more details.

Below is a short summary of some examples of transient method:

- **Transient Plane Source method (TPS)**

In this method a set of concentric ring heaters form the sensor. This bifilar spiral disc is clamped between two identical specimens.

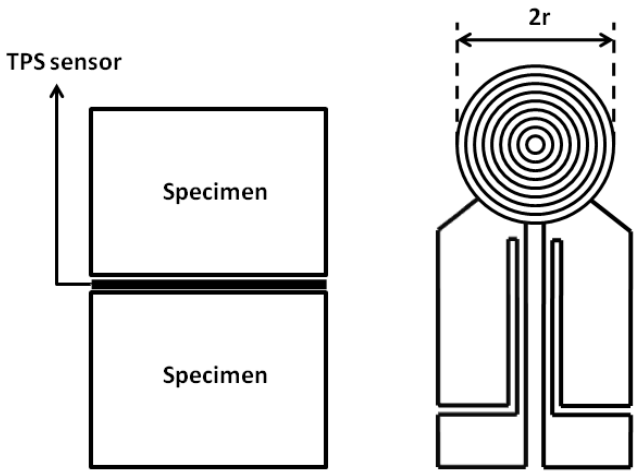

FIGURE 1-2: SCHEMATIC SETUP OF THE TPS METHOD (LEFT), TPS SENSOR (RIGHT)

As the current passes through the TPS sensor (figure 1-2), some heat is generated in between the specimens. It is supposed that the specimens are in thermal equilibrium with surrounding air before proceeding to any measurement. Then, the thermal conductivity of the specimen can be obtained as follows:

$$k = \frac{P_0}{r\Delta T(\tau)\pi^{\frac{3}{2}}} D_s(\tau) \qquad 1\text{-}2$$

Where P_0 is the total output power, $\Delta T(\tau)$ is the mean value of the temperature rise in the TPS element, r is radius of the TPS element and $D_s(\tau)$ is the theoretical expression of the time dependent increase which is considered a design factor of resistive pattern [4].

- **Hot Wire Method**

This method utilizes a linear heat source embedded in the specimen of interest. Then thermal conductivity can be deducted from the resulting temperature rise in a defined distance from this hot wire over a specified time interval. The theory behind this method was developed by Carslaw and Jaeger [5].

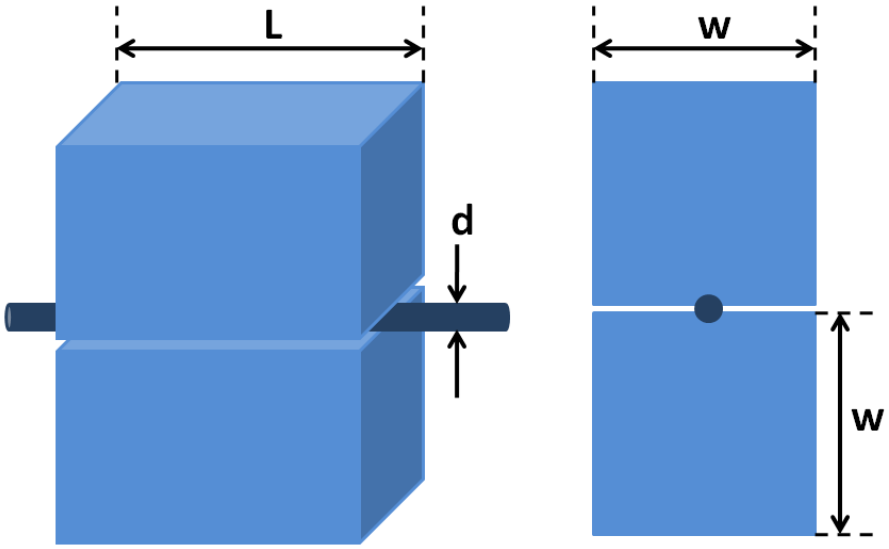

FIGURE 1-3: SCHEMATIC SETUP OF THE HOT-WIRE METHOD (200D<W AND L>4W) [3]

In this method, it is assumed that heat source has a continuous and uniform heat flow along the specimen and specimen itself is isotropic with constant initial temperature. Now the temperature change at the midpoint of the heater is logarithmically plotted against the elapsed time from when the current is flowed through the wire. Then thermal conductivity (k) of the specimen under test can be given as follows [6]:

$$k = \frac{q}{4\pi} \frac{\ln t_2 - \ln t_1}{T_2 - T_1} \qquad 1\text{-}3$$

where q is heat input per unit length of wire, T_1 is the temperature of the line after time t_1 and T_2 is the temperature of the line after time t_2.

- **3-omega measurement technique**

3-omega (3ω) technique was initially suggested by Corbino in 1912 with an aim to study the thermal behavior of metal filaments used in incandescent light bulbs [7]. Then it was developed to measure frequency dependent heat capacity and measuring the thermal diffusivity of liquids [8]. The first application of 3ω method for measuring the thermal conductivity of solids was introduced by Cahill in 1987 [9]. Later on, this method has been investigating for a wide range of materials by other researchers all around the world.

In this method, a micro-fabricated metal strip is deposited on the specimen surface to act simultaneously as a heater and thermometer. By passing an alternating current at angular frequency ω through this strip some heat is created at second harmonic frequency. In turn, it results in temperature change in the heater. Since the electrical resistance of this strip is also influenced by its temperature so the temperature oscillations can be measured indirectly by measuring the 3-omega voltage across the heater and it can also be used to infer the thermo-physical properties of the specimen of interest.

Among different above mentioned approaches of determining the thermal conductivity, the 3-omega (3ω) method possesses some unique advantages. First of all it is capable of accurate measuring the thermal conductivity of a material. Secondly, measurement can be carried out much faster thanks to reducing equilibration time to a few seconds. Thirdly, this method has intrinsically the lowest possible errors caused by blackbody infrared radiation due to substantial reduction in dimension of the heater; For instance, a radiation error of less than 2% even at 1000K [9]. Moreover, it results in the least possible error attributed to contact surface due to evaporating the heater on top of the specimen. This method will be explained in more details in Chapter 3, since it is the method of choice to measure the thermal conductivity of the conducting polymer PEDOT:PSS.

1.3. THESIS STRUCTURE

This thesis work is categorized in seven chapters. Chapter 2 discusses about some fundamental concepts which are necessary to know for later thermal analysis. It also contains primary knowledge around chemical structure of PEDOT:PSS and reasoning of why it is picked up for being thermally characterized. Chapter 3 reviews all analytical background and experimental considerations of 3ω technique to derive formulas for inferring thermal conductivity of the substrate under study. Chapter 4 outlines the procedure steps of specimen preparation. It includes an innovative way of creating a layer of PEDOT:PSS with sufficient thickness and also briefly introduces physical vapor deposition method (PVD) for patterning of heater lines on the specimen surface. Chapter 5 presents the functionalities of various involved instruments and also provides detailed experimental steps of the measurement. Chapter 6 separately depicts and scrutinizes all experimental results obtained from specimens under test. Finally, chapter 7 reviews and makes a conclusion of all findings throughout this diploma work and also creates some horizons for prospective studies in this field of research.

CHAPTER 2

2. THEORETICAL BACKGROUND

The aim for this chapter is to address some fundamental concepts in thermal analysis. It is followed by concise explanation of PEDOT:PSS chemical structure and its properties which is going to be thermally investigated in later chapters.

2.1. HEAT TRANSFER

There are three main ways of heat transfer from one point to another; conduction, convection and radiation. Two first items require a medium for heat to be transferred and they are actually involved in interaction between molecules of a solid or a fluid (gas or liquid). However, radiation heat transfer can take place in vacuum and it is independent of any form of medium. A short description of these ways is given below:

2.1.1. CONDUCTION

It describes the material's ability to let the heat pass through without any motion of material as a whole. The rate of conducted heat is proportional to temperature gradient and intrinsic property of a material called thermal conductivity. This parameter indicates how much heat (in Joule) can be transmitted through one square meter cross section of one meter thick homogeneous material in one second when there is one degree Kelvin temperature difference across the two surface of the material. This is known as Fourier's law and can be formulated as follows:

$$\frac{\Delta Q}{\Delta t} = -kA\frac{\Delta T}{\Delta x} \qquad 2\text{-}1$$

Where $\frac{\Delta Q}{\Delta t}$ is the transported power (W), k is the thermal conductivity of the material ($W.m^{-1}.K^{-1}$), A is the cross section area (m^2) and $\frac{\Delta T}{\Delta x}$ is the temperature gradient ($K.m^{-1}$).

As stated above, the driving force for heat conduction within the materials is inter-molecular motion. As a result, least possible heat conduction is anticipated in vacuum condition due to absence of any molecules for conducting heat. Regarding solids, this phenomenon is explained by the theory of lattice vibrations (phonons). Therefore, diluted materials like gases or amorphous solids are expected to have less value for thermal conductivity compared to most solids. Moreover, metals are better heat conductors than non-metallic solids due to having an abundance of free mobile electrons. These free electrons contribute both in heat and electrical conduction within metals. That is why metals account for both good heat and electrical conductors. However, as the temperature rises, the collision between these mobile electrons acts

as an obstacle against charge transferring. In contrast, the lattice vibration increases by rising in temperature which leads to more heat to be transferred within the metals.

Apart from thermal conductivity, there are two other parameters which need to be taken into account; Thermal diffusivity and specific heat. In fact, these three prominent thermo-physical parameters of each material are correlated with each other as described below:

$$D = \frac{k}{\rho C_p} \qquad 2\text{-}2$$

Where D is defined as thermal diffusivity ($m^2.s^{-1}$), k is the thermal conductivity ($W.m^{-1}.K^{-1}$), ρ is the density ($kg.m^{-3}$) and Cp is the specific heat capacity ($J.K^{-1}.kg^{-1}$) of the material under study. As it is observed in equation (2-2), thermal diffusivity is directly proportional to the value of thermal conductivity and has a reverse dependency to volumetric heat capacity[1] of the material. In other words, it indicates how quickly an input heat can cause rise in temperature within a material rather than it is stored in it.

2.1.2. CONVECTION

This type of heat transfer requires a medium fluid (gas, liquid) to carry heat between the material and another point. There are two types of convection; forced and natural. In forced convection, the fluid is blown or pumped across the material's contact surface and in this way heat can be transferred by this fluid movement. In contrast, no force is used to induce fluid motion in natural convection and a natural repeating cycle of fluid is created around the material due to buoyancy[2]. The amount of transferred heat by convection can be formulated as follows:

$$\Delta Q = h.A.\Delta T \qquad 2\text{-}3$$

Where h is the convective heat transfer coefficient, A is the common surface area between the material and contacting fluid and ΔT is defined as temperature difference between the material and surrounding fluid.

According to equation (2-3), decreasing the contact area between the material and its surrounding fluid or providing the same temperature for material and adjacent fluid can substantially reduce the convective heat transfer.

2.1.3. RADIATION

All objects with a temperature above absolute zero emit thermal radiation. Unlike two above mentioned models for heat transfer, radiation does not require any intermediate substances for heat propagation. Instead, produced heat is transferred by electromagnetic waves or photons mainly in the infrared range. Below is the general formula for calculating of the amount of radiated heat as per Stefan-Boltzmann Law:

[1] Amount of energy needed for increasing the temperature of 1 kg mass of a material by 1 degree centigrade.
[2] Density variation with temperature.

$$q = \varepsilon . \sigma . A . T^4 \qquad 2\text{-}4$$

Where ε is defined as the emissivity of the material, σ is the Stefan-Boltzmann constant which is equal to $5.6703 \times 10^{-8} (W.m^{-2}.K^{-4})$, A is the area of the emitting body (m^2) and T is the absolute temperature of the material (K). Moreover, as a reference, the emissivity of black body is considered one due to the fact that it absorbs all surrounding radiations that fall on its surface without any reflection and emits a broad spectral distribution. As soon as it reaches to adequate level of temperature for emitting energy, one can expect a pure radiation wave without interfering with other reflected ones.

As it is observed in equation (2-4), the most important factor in radiation heat transfer is the absolute temperature of the material to the power four. Therefore, it is possible to greatly diminish the radiated heat losses merely by decreasing the temperature of the material and preferably reducing its surface area.

2.2. THERMOELECTRIC CHARACTERISTICS

Thermoelectric devices are electronic devices in which heat flow and electron flow interfere such that a heat flow can generate an electron flow, or an electron flow leads to a heat flow. Thermoelectric generators produce electricity from temperature difference and thermoelectric coolers transport heat (cool down at one side and heat up at the other side) when a current pass through them. Those thermoelectric effects consist of three thermodynamically reversible effects, Seebeck effect, Peltier effect and Thomson effect. Although, these effects are not independent of each other but two latter ones (Peltier and Thomson effects) are not in the scope of this work. Below is an introduction on the Seebeck effect and the dimensionless figure-of- merit as two material properties relevant for thermoelectric generators.

2.2.1. SEEBECK EFFECT

The main concept of thermoelectric power generation is based on the Seebeck effect. It explains how a voltage (moving charge carriers) is built up in metals or semiconductors due to a temperature gradient applied on their both sides. The theory behind this phenomenon is explained by Thomas Johann Seebeck (1770-1831). He was the first physicist who came up with the idea of generating a magnetic field when two different metals are connected in series on condition that two junctions are kept at various temperatures. Although he primarily observed the magnetic field and interpreted it due to temperature difference but later, thanks to Danish physicist Hans Christian Orsted (1777-1851), he realized that an electrical current is induced in the circuit and it actually causes a magnetic field to be created around the metal conductors.

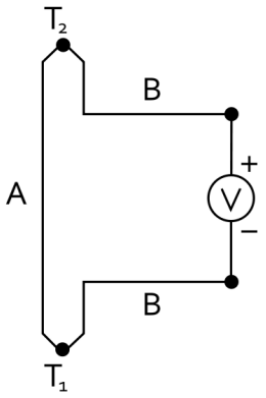

FIGURE 2-1: SCHEMATIC FIGURE SHOWING THE SEEBECK EFFECT

This phenomenon is clarified by two effects; charge carrier diffusion and phonon drag. These two effects explain how temperature gradient makes electrical current (moving charge carriers) within material. The greater the temperature difference the greater the induced voltage. Here is general formula for induced voltage:

$$V = \int_{T_1}^{T_2} \big(S_B(T) - S_A(T)\big) dT \qquad 2\text{-}5$$

Where, S_A and S_B are the Seebeck coefficients of material A and B respectively. Seebeck coefficient or thermoelectric power of a material is defined as a scale to quantify the amount of induced voltage per temperature difference. This parameter is greatly dependent on material's temperature and its morphological structure and most importantly in the density of charge carriers in the material. In practice, the Seebeck coefficient is typically in a range of few micro volts per Kelvin ($\frac{\mu V}{K}$) for metals up to millivolts per Kelvin for insulators.

2.2.2. FIGURE OF MERIT

The figure-of-merit is considered as a benchmark for determining how suitable a material is to be employed for thermoelectric application. In other words, the higher the figure of merit, the higher the efficiency of using that material for thermoelectric purposes. It is defined as follows:

$$Z = \frac{\sigma S^2}{k} \qquad 2\text{-}6$$

Where S is Seebeck coefficient, σ is the electrical conductivity and k is the thermal conductivity of the material under study. Moreover, the numerator of equation (2-6) is known as the power factor (σS^2). The dimension of the figure of merit is derived as the reverse of temperature in Kelvin (T^{-1}). In order to introduce a dimensionless figure of merit (ZT), it is required to simply multiply it by the average absolute temperature at which the measurement is taken.

As it is concluded from equation (2-6), in order to maximize the dimensionless figure of merit and consequently improve the thermoelectric properties of a material, it is required that following actions to be taken simultaneously:

- Maximizing the thermoelectric power (Seebeck coefficient, S)
- Maximizing the electrical conductivity (σ)
- Minimizing the thermal conductivity (k)

According to Slack et.al, a novel thermoelectric material needs to possess electronic properties of a crystalline material and the thermal properties of a glass [10]. However, the highest value for ZT has been around one for more than three decades without any theoretically proof to explain why it cannot be improved further. However, recently by introducing new generation of semiconductors including nanostructures to enhance phonon scattering, the thermal conductivity has been diminish significantly thus leading to unprecedented high ZT values (between 2 and 3 or even higher [11]). By applying new types of thermoelectric materials, it is possible to fully meet above mentioned requirements and introduce genuine choices for power harvesting purposes such as waste heat recovery. The interesting point with conducting polymers is their expected intrinsic low thermal conductivity as they resemble traditional plastic known as thermal insulators.

2.3. PEDOT:PSS

Poly (3, 4-ethylenedioxythiophene) or PEDOT is one of the most widely used π-conjugated polymers. Films of this conducting polymer (CP) are optically transparent in their conducting state. Despite having lots of positive charges (absence of electron), as its name p-type, the doped polymer is quite stable and reluctant to be reduced; i.e. exhibit low tendency to obtain electron. Because of this combination of properties, PEDOT has been used as plastic transparent electrodes in organic-based optoelectronic applications, but also as antistatic films.

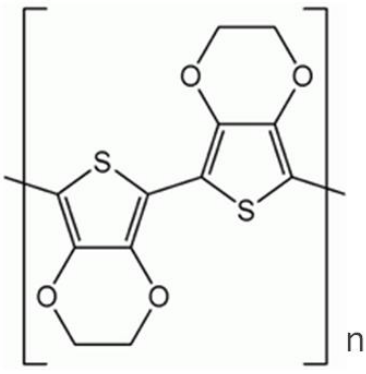

FIGURE 2-2: SCHEMATIC OF PEDOT CHEMICAL STRUCTURE

In order to enhance the solubility of PEDOT, it needs to be mixed with poly (styrenesulfonic acid) (PSS) with different concentration. The combination known as PEDOT:PSS. In our case, the concentration of PSS ingredient in the polymer blend is up to 70%. In water, the polymer blend PEDOT:PSS is stable as a suspension of PEDOT:PSS nanoparticles.

The solution processability, the electrical conductivity and likely its relatively low thermal conductivity are properties that make this organic semiconductor an interesting material for thermoelectricity.

CHAPTER 3

3. ANALYTICAL REVIEW

In order to have a better understanding of the 3ω technique, it is crucial to have a consolidate knowledge about basic model and the parameters which influence the output data. This section explains all the analytical background behind the 3ω technique.

Figure (3-1) depicts a sample heater/thermometer which is deposited on the specimen of interest.

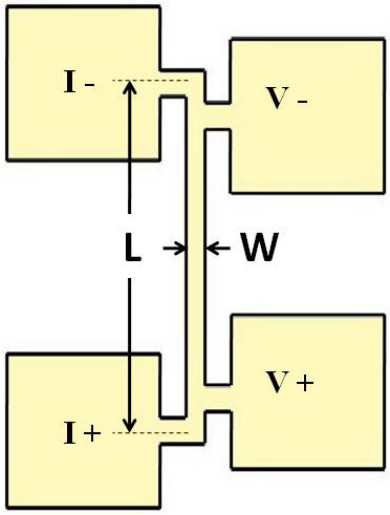

FIGURE 3-1: SCHEMATIC FIGURE OF HEATER

It is composed of four pads connected through a narrow line. The outer pads are used for connecting probes to make a close circuit and the inner ones are employed for measuring the electrical potential difference across the heater/thermometer. Depending on the length of the line (L) and also its width (w), different resistance and subsequently various voltages can be measured by passing a constant amount of current. This is explained by Ohm's law for a uniform conductor as stated below:

$$R = \rho \frac{L}{A} \qquad 3\text{-}1$$

Where L and A are the length (m) and the cross-sectional area (m^2) of the conductor respectively and ρ is the static resistivity (Ω.m).

To commence, consider an alternating current of frequency of ω passing through the heater/thermometer; from now on referred to as the heater. It is given as:

$$I_{h,0}(t) = I_{h,0} \cos(\omega t) \qquad 3\text{-}2$$

Where $I_{h,0}$is the peak amplitude of the nominal heater current at a frequency ω and $I_{h,0}(t)$ is the instantaneous current passing through the heater.

This current generates heat according to Joule heating as stated below:

$$P_h(t) = I_{h,0}^2 R_{h,0} \cos^2(\omega t) = \frac{1}{2} I_{h,0}^2 R_{h,0}(1 + \cos(2\omega t)) \quad 3\text{-}3$$

Where $R_{h,0}$ is the nominal heater resistance and $P_h(t)$ is the instantaneous produced power by the heater measured in Watt (W). As it is observed, the instantaneous power can be split into two components; firstly the power attributed to the direct current (P_{DC}); and secondly, the alternate current power (P_{AC}).

$$P_{DC} = \frac{1}{2} I_{h,0}^2 R_{h,0} = \frac{1}{2} P_{h,0}(t) \quad 3\text{-}4$$

$$P_{AC} = \frac{1}{2} I_{h,0}^2 R_{h,0} \cos(2\omega t) \quad 3\text{-}5$$

Here, it is useful to introduce the root mean square (RMS) of power per unit heater length for further replacements. It is equivalent of power dissipated by direct current of the same amplitude and can be defined as follows:

$$P_{rms} = I_{h,rms}^2 R_{h,0} = P_{DC} \quad 3\text{-}6$$

Where $I_{h,rms}$ is the mean root square of the current given by:

$$I_{h,rms} = \sqrt{\frac{1}{\tau} \int_0^{\tau} I_{h,0}^2(t)\, dt} = I_{h,0} \sqrt{\frac{\omega}{2\pi} \int_0^{\frac{2\pi}{\omega}} \cos^2(\omega t) dt} = \frac{I_{h,0}}{\sqrt{2}} \quad 3\text{-}7$$

Where τ is the required time for one cycle of the applied sinusoidal current.

This power generates the temperature change in the heater and the underneath substrate. This temperature difference is also constituted of direct and alternate components as follows:

$$\Delta T = \Delta T_{DC} + |\Delta T_{AC}| \cos(2\omega t + \varphi) \quad 3\text{-}8$$

If the substrate is insulating, the heat stays in the heater and the temperature oscillation is large. Hence, measuring this temperature oscillation allows accessing the thermal properties of the underneath substrate. To measure this temperature oscillation, one can measure the resistance of the heater and use the heater also as a temperature sensor. Moreover, the resistance of the heater varies with temperature. It is given by:

$$R = R_0(1 + \beta_h \Delta T) \quad 3\text{-}9$$

Where β_h is the temperature coefficient of resistance (TCR) of the heater and R_0 is the resistance value at temperature T_0. It is worth mentioning that there is a difference between the rate of the

resistivity change versus temperature ($\frac{dR}{dT}$) and TCR value; although they are proportional but they should not be mistaken by each other as stated below:

$$\beta_h = \frac{1}{R_0}\frac{dR}{dT} \qquad 3\text{-}10$$

By merging the equations (3-8) and (3-9), the general formula for resistance of the heater can be derived as follows:

$$R_h(t) = R_{h,0}(1 + \beta_h \Delta T_{DC} + \beta_h |\Delta T_{AC}| \cos(2\omega t + \varphi) \qquad 3\text{-}11$$

Now, to measure the resistance of the heater, the voltage drop across the heater must be measured. The expression of this voltage is given by multiplying equations (3-2) by (3-11) as follows:

$$\begin{aligned} V_h(t) = I_{h,0}R_{h,0}\Big[&(1 + \beta_h \Delta T_{DC})\cos(\omega t) + \tfrac{1}{2}\beta_h |\Delta T_{AC}| \cos(\omega t + \varphi) \\ &+ \tfrac{1}{2}\beta_h |\Delta T_{AC}| \cos(3\omega t + \varphi)\Big] \end{aligned} \qquad 3\text{-}12$$

In equation (3-12), it is clearly observed that the last voltage component is oscillating at third harmonic frequency. The magnitude of third harmonic voltage is typically 1000 times smaller than that of the first harmonic voltage [9] and also contains useful information about thermal conductivity of the underneath specimen. It is given by:

$$V_{h,3\omega} = \frac{1}{2}V_{h,0}\beta_h \Delta T_{AC} \qquad 3\text{-}13$$

Where $V_{h,0}$and $V_{h,3\omega}$ are the peak amplitude of the nominal heater voltage at first and third harmonic frequency respectively. Notice that ΔT_{AC} and $V_{h,3\omega}$ are complex numbers which are composed of in-phase and out-of phase components as follows:

$$V_{h,3\omega} = V_{h,3\omega,x} + iV_{h,3\omega,y} \qquad 3\text{-}14$$

$$\Delta T_{AC} = \Delta T_{AC,x} + i\Delta T_{AC,y} \qquad 3\text{-}15$$

Moreover, as it is observed in equation (3-13), the temperature difference between heater and the underneath substrate is proportional to third harmonic voltage change of the heater itself. It is of great importance to note when these two parameters are replaced by each other in the derived formula at the end.

3.1. 1D HEATER DEPOSITED ON THE SPECIMEN

In this section, some theoretical assumptions are made to find the interrelation between the produced heat and thermal conductivity of the substrate.

First of all, it is supposed that there is an intimate contact between heater and underneath substrate. Then, for facilitating the calculation, an infinite 1D heater is considered. It causes a cylindrical temperature profile around the heater line. However, half of this profile is taken into

consideration assuming there are not any forms of heat transfer (conduction, convection and radiation) on the contact side with air.

Here is the heat conduction equation through semi-cylindrical temperature profile. Notice that there is only a radial temperature gradient.

$$P_h(t) = -k_s A_r \frac{dT_{AC}(r)}{dr} \quad 3\text{-}16$$

Where k_s is the thermal conductivity of the specimen, A_r is the peripheral area of the heat flow profile (surface area of a half cylinder).

$$A_r = \pi r l_h \quad 3\text{-}17$$

Now we can infer a general formula for radial temperature gradient caused by a deposited 1D heater line on top of the substrate of interest.

$$P_h \int_{r_1}^{r_2} \frac{dr}{r} = -k_s \pi l_h \int_{T_1}^{T_2} dT_{AC}(r) \quad 3\text{-}18$$

$$\Delta T_{AC}(r) = -\frac{P_h}{k_s \pi l_h} \ln \frac{r_2}{r_1} \quad 3\text{-}19$$

As it is observed in equation (3-19), the lower the thermal conductivity of the substrate, the higher the temperature differs in distance r from the heater source. By merging two equations (3-19) and (3-13), one can derive a general formula for thermal conductivity of specimen in case of some measurable parameters attributed to the heater. It is necessary to mention that twice of equation (3-13) is considered because there is no temperature gradient within half of the considered cylinder and all input power result is twice temperature increase of the specimen underneath. Here it is:

$$k_s = \frac{V_{h,0}^3 \ln \frac{f_2}{f_1}}{4\pi l_h R_{h,0}^2 \left(V_{3\omega,1} - V_{3\omega,2}\right)} \frac{dR}{dT} \quad 3\text{-}20$$

Where $V_{3\omega,1}$ and $V_{3\omega,2}$ are the third harmonic voltage at input current frequency of f_1 and f_2 respectively. Also $\frac{dR}{dT}$ is the rate of resistance change of the heater with its temperature variation as already discussed. Notice that the radial distance (r) is replaced by applied frequency (f) due to the fact that they are reversely proportional to each other as stated in following:

$$r = \left|\frac{1}{q}\right| = \sqrt{\frac{D}{4\pi f}} \quad 3\text{-}21$$

Where $\frac{1}{q}$ is the thermal penetration depth which is the maximum depth of heat diffusion caused by input frequencies (f) and D is the thermal diffusivity of the specimen.

Equation (3-20) can also be written in following form by putting TCR value of the heater (β_h):

$$k_s = \frac{V_{h,0}^3 \beta_h}{4\pi l_h R_{h,0} S} \qquad 3\text{-}22$$

Where S is defined as the slope of the linear section in the graph of the overall third harmonic voltage amplitude versus natural logarithm of the applied frequencies.

In order to precisely distinguish the linear region, it is required to meet two following requirements:

- There should be a linear relation between the overall third harmonic voltage amplitude in a logarithmic scale plot
- The magnitude of out-of-phase third harmonic voltage should have a constant value

The following section provides a detailed explanation of the different regions attributed to the specimen, which are influenced by the generated heat of the heater.

3.2. 2D HEATER DEPOSITED ON THE SPECIMEN

This is just a modification of previous section to make it more feasible by converting to real life cases. In this regard, some theoretical assumptions are made for extracting relevant formulas. However, it is not aimed at going through these mathematical calculations; instead, some helpful consequences are addressed in the following.

In this regard, considering a 2D heater seems to be a nice approximation of a heater behavior. Therefore, heater dimension should be selected in a way that its length and width magnitude would be much greater than its thickness ($l_h \gg w_h \gg t_h$). It requires us to deposit an infinite number of 1D heaters on the surface of the specimen. In our case, the length, width and thickness of the heater are in a range of some mm, µm and nm respectively.

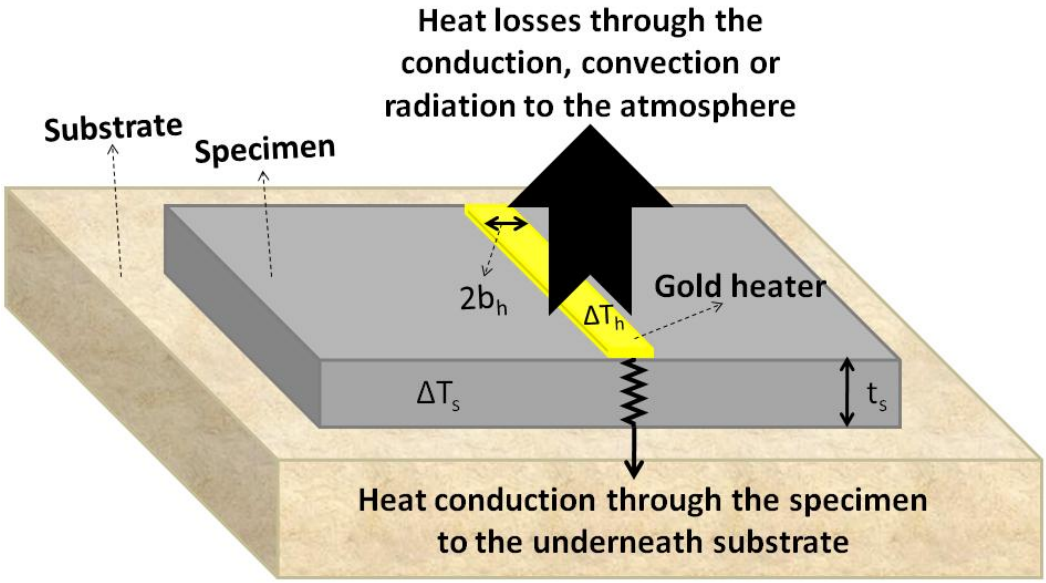

FIGURE 3-2: SCHEMATIC FIGURE OF SPECIMEN WITH ALL HEAT FRACTIONS

As shown in figure (3-2), the produced heat caused by passing an alternating current through the heater can be split into three different parts.

The first part is the heat losses to the atmosphere through conduction, convection and radiation. Although, the latter one constitutes the predominant part of heat losses since conduction and convection heat losses to the atmosphere can be dramatically diminished by carrying out measurement in vacuum condition. Moreover, minimizing the heater dimension and decreasing working temperature (few degrees above room temperature) are two effective ways of decreasing the heat losses through radiation. Therefore, this part can be ignored in our calculations.

The second part is the heat generating the temperature difference in the specimen and the heater itself. It should be noted that the specimen and the deposited heater are considered as a single system so prior to connecting the current they have the same temperature but after passing the current the produced heat in heater results in a uniform temperature difference in heater due to assuming a 2D heater. In contrast, there is a temperature gradient along the thickness of the specimen. Therefore, the heat waves and the temperature difference vary with current frequency. In this way, the specimen thickness is separated into three main regions, as explained below.

The last part of the produced heat is conducted through the specimen to underneath substrate. This is considered an inevitable heat loss but it can be minimized by using a low thermal conductor material as underneath substrate.

According to equation (3-19), and introducing the parameter b_h (half-width of the heater) as a benchmark for the amount of heat penetration depth, one would be able to divide the heat affected region of the substrate into three distinct parts known as planar, transition and linear regions [13].

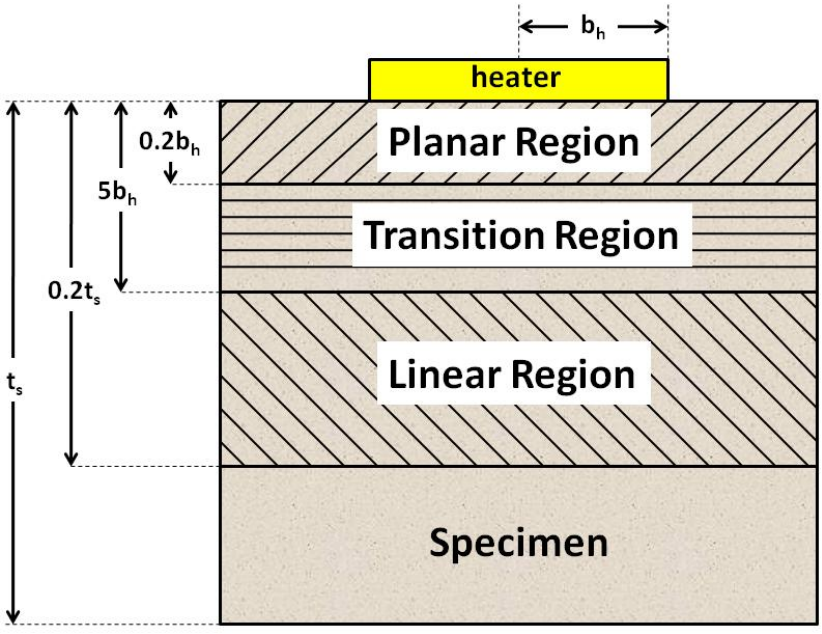

FIGURE 3-3: CROSS VIEW SECTION OF SPECIMEN (NOT TO SCALE)

3.2.1. PLANAR REGION

This volume is restricted on one hand to near the surface of the specimen ($0.01b_h$) and one the other hand to one fifth of the heater half-width with assuming a maximum RMS error of 0.15% [14].

In this volume, the absolute magnitudes of in-phase and out-of-phase components of the temperature oscillation are equal but there is a 45 degrees phase lag between them. Moreover, the temperature variation between heater and any points in this region is quite small and approaches to zero due to having a shallow penetration depth.

3.2.2. LINEAR REGION

In order to minimize heat losses, it is necessary not to heat our sample beyond a certain level. Therefore, there is a limit for heat penetration depth and in turn for minimum applied frequency. On the contrary, there is also upper limit for frequency attributed to minimum penetration depth. It should be selected in a way that it passes nonlinear region near the surface.

The boundary for linear region is defined in a range between five times the half-width of the heater ($5b_h$) and one fifth of the specimen thickness ($0.2t_s$). This assumption is regarded as a nice approximation of considering a semi-infinite specimen and includes only a maximum RMS error of 0.25%. This error can be decreased to about 0.02% by changing the lower limit of linear region to 40 times of the half-width of the heater [14].

The in-phase component of the temperature oscillation between heater and any points in this region decreases logarithmically (linearly against logarithm of frequency) by enhancing the thermal excitation frequency. In contrast, the imaginary part of the temperature oscillation over the same frequency interval exhibits a constant negative value.

3.2.3. TRANSITION REGION

This region indicates the area which separates the above mentioned two sections. Conversely to constant negative value for out-of-phase temperature oscillation in linear region, this component varies in transition region. While, there is still a logarithmic decrease for in-phase temperature oscillation with the same slope as the linear section.

3.3. APPROXIMATE CALCULATION OF FREQUENCY INTERVAL OF LINEAR REGION

As stated in previous section, there are boundary limits for the amount of heat diffusion through the specimen provided that it is kept in linear region. For this purpose, one can conclude an upper/lower boundary for the amount of excitation frequency. Here is another form of equation (3-21) in terms of heat penetration depth (r).

$$f = \frac{D}{4\pi r^2} \tag{3-23}$$

According to the boundary restrictions of linear region, the upper/lower limits for this region can be chosen as:

$$r_{min} = 5b_h \tag{3-24}$$

$$r_{max} = 0.2t_s \tag{3-25}$$

Where, b_h and t_s are half-width of the heater and the thickness of specimen respectively.

Therefore, the excitation frequency lies in the range as defined in below:

$$\frac{100D}{16\pi t_s^2} \leq f_{linear} \leq \frac{D}{100\pi b_h^2} \tag{3-26}$$

This is a rough estimation of the frequency limits to define the linear region in order to derive the parameter *S* (slope of the linear section) which was already explained. It can also be concluded that the linear region for materials with high thermal conductivity (and also high thermal diffusivity) occurs in higher frequencies than that of low thermal conductors provided the values for both thickness of specimen (t_s) and half-width of the heater (b_h) remain constant. It can be considered as a basis for materials with unknown characteristics. This will be further discussed in chapter 5 for adjusting the upper limit frequency to balance the Wheatstone bridge at fundamental voltage signal.

It is also worth mentioning that it is possible to derive the minimum thickness (t_s) of specimen by merging upper/lower limits of linear region frequency. As it is observed in equation (3-26) the upper limit for linear frequency band is decreased by increasing the half-width of the heater (b_h). Therefore, the minimum thickness of the specimen is dependent upon the half-width of the heater and should satisfy the following requirement.

$$t_s \geq 25b_h \tag{3-27}$$

Hence, it is recommended that specimen thickness is selected in a range between 1mm to 5 mm provided that the half-width of the heater (b_h) do not exceed 40 micron.

CHAPTER 4

4. SPECIMEN PREPARATION

The specimens which are being used in this work are ordinary window glass, Sialone® and PEDOT:PSS. As discussed in previous chapter, the minimum required thickness for the specimen of interest can be roughly estimated by equation (3-27) considering the fact that the least possible heater half width (b_h), in our case, is around 10 microns. So the minimum attributed thickness for the specimen should be equal to 250 microns. In case of glass and Sialone®, this parameter does not make any problem since they are available at any desired thicknesses. However, the later specimen (PEDOT:PSS) is in liquid state and it is a great challenge to create such thick layer of this conducting polymer. Moreover, it needs to have as smooth surface as possible for further heater deposition process to avoid interface heat scattering. We describe hereafter an innovative way to create a PEDOT:PSS layer.

4.1. CREATING PEDOT:PSS LAYER

The thick layer (around half a millimeter) of PEDOT:PSS will be fabricated from a PDMS mould. There are two reasons for selecting PDMS; first, the resulting mould will have a quite flat surface which is a necessity for further processing steps. Secondly, there is poor adhesion between PDMS and PEDOT:PSS; which is a great advantage when PEDOT:PSS is peeled off from the mould.

In following, we described the fabrication steps of the PDMS mould.

4.1.1. INITIAL PREPARATION

In order to minimize every possible contamination of other instruments with PDMS, it is strictly advised not to work with the same glove for mould making as doing other tasks. Therefore, one extra pair of gloves, a plastic glass and spoon and also a plastic bag for disposing of all wastes are required prior to start mould making.

4.1.2. MAKING THE MIXTURE

The mixture is a combination of PDMS prepolymer "base"[3] and a "curing agent"[4] of Dow Corning Sylgard 184 with proportionality of 10:1 [15]; e.g. in our case, 30 gram of base is mixed

[3] The base comprises a platinum catalyst dissolved in a T-type vinyl-terminated poly(dimethyl)-siloxane (PDMS) and D-level PDMS prepolymers.
[4] The curing agent is a vinyl-terminated poly(dimethyl)-siloxane and trimethylsiloxy-terminated poly(methylhydrosiloxane) prepolymer.

with 3 gram of curing agent. Then it needs to be rigorously stirred up to have a homogenous mixture at the end.

4.1.3. DEGASIFICATION

This step aims at removing the dissolved air in the mixture. It can be accomplished by simply putting the mixture inside the vacuum chamber for almost one hour. If needed, it can be kept longer inside vacuum chamber to remove all air bobbles and prevent from any possible unwanted cavitations on the inner side of the mould surface.

4.1.4. FORMING DESIRED MOULD SHAPE

The object of desired thickness is put in a plastic vessel and the PDMS mixture is poured inside the glass to encompass the object in all directions. Now, it needs a while to get hard. In order to accelerate this process, it can be kept at 60 degrees centigrade in the oven for an hour. After baking the mould, it is removed from plastic vessel.

A photograph of the mould is shown in figure 4-1. The squared shape cavity will be filled by the water suspension of PEDOT:PSS.

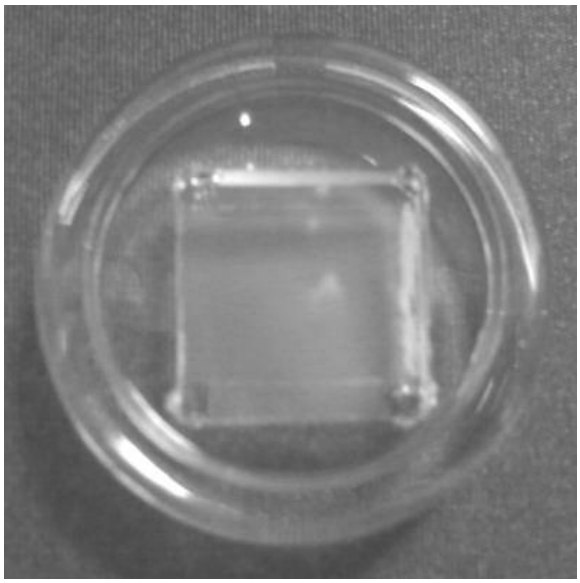

FIGURE 4-1: PDMS MOULD FOR CREATING PEDOT:PSS LAYER

4.1.5. MAKING PEDOT:PSS LAYER

Now, to get a solid pellet, PEDOT-PSS solution is poured inside the mould and the solvent gradually evaporates. This process takes a couple of days to obtain the desired thickness, although, it could be facilitated by putting inside the oven and setting the temperature to at most 50-60 (^{o}C).

4.2. HEATER PATTERNING BY SHADOW MASK

Using shadow mask is the most precise and also the quickest approach for patterning metal strips on the specimen of interest. This method enables us to create quite uniform strips as narrow as 10 μm without any need to do photolithography process. It specially plays a vital role in case of PEDOT:PSS which is soluble material and degrades during the photolithography process.

The figure below shows two different patterns of shadow mask which were used in this work.

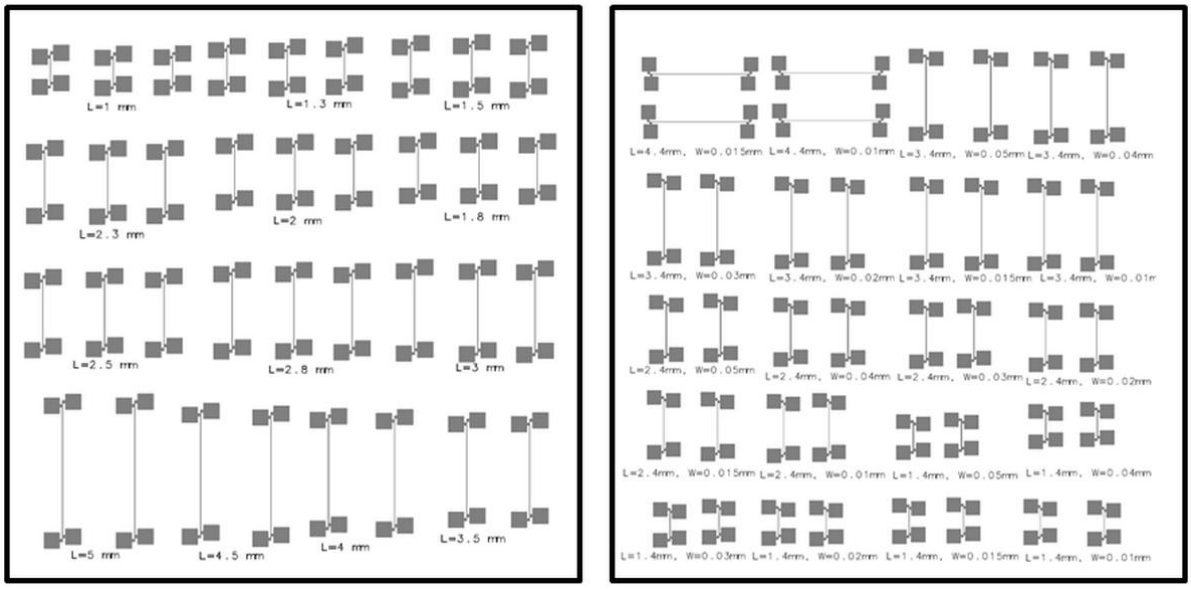

FIGURE 4-2: TWO DIFFERENT PATTERNS OF SHADOW MASK WITH VARIOUS LENGTH AND WIDTH FOR DEPOSITED HEATER

The metal stripe needs to fulfill specific requirements. The metal stripe acts as a heater and a thermometer and should not be easily oxidized. Moreover, since the temperature variation is relatively small (few degrees), it is necessary that the selected metal possesses a resistance that varies significantly with the temperature. Gold can fully meets all these requirements accompanying some other unique characteristics. First, its resistivity is quite well sensitive to temperature oscillations (especially for above room temperature) and even a minor temperature variation can have a remarkable effect on its resistivity. Moreover, gold is not vulnerable to oxidation and also it is both less expensive and scarce than other possible candidates like platinum.

In order to improve the adhesion between gold and the specimen under study, a layer of chromium with thickness almost one tenth that of gold is applied in between. Therefore, it can be neglected in our measurements due to its small dimension.

The deposition of gold/chromium on the observed specimen surface is accomplished in a Balzers BA510 evaporator. The physical vapor deposition (PVD) is done in vacuum condition with pressure of about $5x10^{-5}$ Torr. Vacuum condition prevents any deflection of particles directions towards the target pattern.

FIGURE 4-3: PICTURE OF THE BALZERS BA510 EVAPORATOR

It is important to note that prior to any evaporation, it is required to properly clean the surface. This is simply performed by ultrasonic cleaning of the specimen in acetone followed by isopropyl alcohol and distilled water. These cleaning processes together with the chromium layer ensure a good adhesion of the heater on the specimen.

In order to start evaporating, first of all, chromium (Cr) and gold (Au) are loaded in separate Tungsten (W) boats (having a high melting point). Then, the next step is pumping down the chamber. It normally takes at least 2 hours to reach the appropriate pressure (around $5x10^{-5}$ Torr). However, it is advised to pump down over night to have the most ideal vacuum condition.

Now the evaporation process can start. It is performed by driving a current through electrode bases of the boats. As the current is gradually increased by clockwise turning of the evaporation power handle, it results in heating up of the boat and its contents. While the melting point for boat is much greater than its contents so passing current just causes melting and evaporation of chrome and gold. This melting can be easily observed during evaporation process by emitted light. This process starts with chromium and continues with gold particles. However, it is advised to have simultaneously evaporation of gold and chromium in last few angstrom thickness of chromium layer prior starting the gold evaporation such that the metals mix in some region to finish with a pure gold film on the top.

The thickness of deposited layers is controlled by a digital deposition monitor (INFICON, model XTM) which has been already set to the suitable program of the material under evaporation.

Other detailed information for gold and chrome deposition can be found in following table 1.

TABLE 1: DETAILED INFORMATION FOR GOLD AND CHROME DEPOSITION

Material	Current (A)	Thickness (Å)	Deposition rate (Å/s)
Chrome	9 - 11	100 - 200	0.5 - 1
Gold	5-7	1500 - 2000	2 - 3

The last important point to mention is that the shadow mask should be placed between the two boats in order to prevent any shadow effect[5].

[5] Deposition of gold adjacent to the chrome layer rather than to be on top of it.

CHAPTER 5

5. IMPLEMENTATION OF THE 3-OMEGA TECHNIQUE

There are two independent measurements which need to be carried out in order to find the thermal conductivity of the specimen. The 3-omega voltage to estimate the temperature oscillation and the variation of resistance of the heater vs. temperature. The results of the following two measurements are used as input data for equation (3-22). Here is a detailed explanation of these two measurements.

5.1. 3-OMEGA MEASUREMENT

This section is divided into two parts; first, a brief description of all required instruments which are used for implementing of 3ω measurement technique and the second part provide a detailed procedure of experimental steps.

5.1.1. EXPERIMENTAL APPARATUS

- **Lock-in Amplifier**

Since the 3ω voltage is normally 1000 times smaller than the fundamental voltage (7), the signal needs to be amplified. Lock-in amplifier is specially designed to serve this purpose. It is able to detect and measure very minute AC signals in the range down to a few nanovolts in the presence of large amount of noise.

The technique in use is called phase-sensitive detection (PSD) to separate the components of the input signal at a specific reference frequency and phase. Also, all other noise signals at frequencies other than the reference frequency are neglected.

An ideal amplifier yields a noise signal about 5 nV per root of amplifier bandwidth frequency. Therefore, in order to precisely measure the very small input signal with the least possible uncertainty, it is required to attenuate noise by narrowing the bandwidth of the input signal to about 0.01 Hz. This is achieved through the combination of the phase-sensitive detector and a low pass filter. Here is an explanation of how this technique works.

Assuming a reference signal that is generated either internally by lock-in internal oscillator or externally through a function generator. The experiment is excited by this reference sinusoidal signal and the response is defined as follows:

$$V_{ref} = V_{sig}\sin(\omega_r t + \theta_{sig}) \quad 5\text{-}1$$

Where V_{sig} is the signal amplitude and ω_r and θ_{sig} are reference frequency and signal phase respectively.

Sine waves of different frequencies are orthogonal to each other. In other words, the average of the product of two sine waves would not be zero if and only if their frequencies are exactly the same. As a result, if the response signal from the experiment is multiplied by a pure signal generated by the lock-in amplifier given as$V_L\sin(\omega_L t + \theta_{ref})$ then the product would be:

$$V_{psd} = V_{sig}V_L\sin(\omega_r t + \theta_{sig})\sin(\omega_L t + \theta_{ref}) \quad 5\text{-}2$$

$$V_{psd} = \frac{1}{2}V_{sig}V_L[\cos([\omega_r - \omega_L]t + \theta_{sig} - \theta_{ref}) - \cos([\omega_r + \omega_L]t + \theta_{sig} + \theta_{ref})] \quad 5\text{-}3$$

Where V_{psd} is the amplitude of phase sensitive detector. As it is observed in equation (5-3), by adjusting the lock-in frequency same as the reference one ($\omega_r = \omega_L$) and also applying a low pass filter, the product yields a DC output signal as follows:

$$V_{psd} = \frac{1}{2}V_{sig}V_L\cos(\theta_{sig} - \theta_{ref}) \quad 5\text{-}4$$

The low pass filter actually eliminate both the 2f (sum of ω_r and ω_L) and the noise components. It can be accessed by setting the time constant. The time constant is defined as follows:

$$TC = \frac{1}{2\pi f} \quad 5\text{-}5$$

Therefore, another important matter is to adjust a suitable time constant value for each measurement. According to equation (5-5), the time constant is inversely proportional to the applied frequency (TC~f^{-1}). In other words, if the input signal frequency is set to e.g. 0.1 Hz, then the proper time constant should be adjusted to 10 (s). Otherwise, the value of X and Y (in-phase and out-of-phase components) would become noisy because the noisy signal is no longer attenuated completely by the low pass filters. Interesting to note is that for frequencies below 200 Hz, one can take advantage of the synchronous filter to remove the 2f component of the output without using a long time constant.

Moreover, in order to pick out a DC output signal proportional to the signal amplitude, not only do the frequencies need to be the same but the phase difference between these two signal should not change otherwise the product would be no longer a DC signal. For this purpose, the internal generated signal is locked, hence the name: lock-in amplifier, to the external reference and in this way it can continuously track it.

Here, a dual phase digital lock-in amplifier, Stanford Research System model SR850, is being used. The only difference with a single phase lock-in is having two PSD's, with 90 degrees phase difference. It can simultaneously measure X, Y, R and θ as described below:

$$X = V_{sig}\cos\theta \quad 5\text{-}6$$

$$Y = V_{sig} \sin\theta \quad (5\text{-}7)$$

$$R = \sqrt{X^2 + Y^2} = V_{sig} \quad (5\text{-}8)$$

$$\theta = \tan^{-1}\left(\frac{Y}{X}\right) \quad (5\text{-}9)$$

Where θ is defined the phase between the signal and lock-in reference.

- **Function Generator**

This instrument provides reference signal both as an external oscillator for lock-in amplifier and also for stimulating the circuit under study. Here, an arbitrary waveform generator (Agilent model 33250A) was used for this purpose.

FIGURE 5-1: FRONT PANEL VIEW OF AGILENT TECHNOLOGIES 33250A ARBITRARY FUNCTION GENERATOR

This model of function generator is able to create sine, square, ramp, noise or any other desired waveforms with frequency range between 1 μHz and 80MHz. Magnitude of signal frequency, amplitude and offset can be adjusted either by symmetric dial or entering the value by numeric keypad.

- **Cryogenic Probe Station**

The 3ω measurements are carried out inside Cryogenic probe station. The micro-manipulated probe station being used here is Janis (Model, ST-4LF-2MW-2-CX). It is a continuous flow cryogenic system which is equipped with four micro-manipulated probes each has three degrees of freedom. To reduce noise, some wires with BNC jack labeled connectors are required for connecting these probes to other measuring devices. In addition, it is supplied with a microscope to provide better view for precise manipulation of the probe tips on the specimen surface. An adjustable fiber-optic light pipes is also included for illuminating of the surface under test. This tabletop model is mounted on a base to eliminate any vibration and provide the most stable position for the specimen.

FIGURE 5-2: CRYOGENIC MICRO-MANIPULATED PROBE STATION, MODEL ST-4LF-2MW-2-CX WITH OPTICS

The operating temperature is in a range of 6-450(K) which is monitored by a controller (model 9700) equipped with two temperature sensors; one is mounted on the cold finger of the cryostat and the other is located in mounting plate inside the vacuum chamber. The controller makes equilibrium between liquid nitrogen source (LN_2) and the heater input power to provide a stable temperature at any set point adjusted by the user.

- **Wheatstone Bridge**

Wheatstone bridge is a circuit for measuring an unknown electrical resistance which is composed of two legs including four resistances, two per each leg. In our case, the gold heater (R_h) in series with another resistance (R_1) is configured as one leg. The other leg is comprised two resistances R_2 and R_3 while a variable resistance is in parallel with resistance R_2 as it is depicted in figure (5-3).

It can be shown that when the following relation is satisfied between resistances then no current would flow through the connection line between two legs. It can be reached by adjusting the variable resistance R_2.

$$\frac{R_h}{R_1} = \frac{R_3}{R_2} \qquad 5\text{-}10$$

Despite requiring to meet the above condition, there are also two other important requirements to measure the 3ω voltage of the heater. Firstly, the most part of the current needs to pass through the leg containing the gold heater. To do so, the resistance R_3 is selected much larger than the heater resistance. For instance, if the value of resistance R_3 would be 1000 times of the heater resistance then less than 0.1% of the current flows through the R_3 in case of balanced Wheatstone bridge. Secondly, to prevent any spurious 3ω voltage result from resistance R_1 which is in series with heater, it needs to have high power rating.

It can be shown that the measured third harmonic of the Wheatstone bridge output ($W_{3\omega}$) is proportional to the 3ω voltage of the heater as follows:

$$V_{h,3\omega} = \frac{R_h + R_1 + R_A}{R_1 + R_A} W_{3\omega} \qquad 5\text{-}11$$

As it is observed in equation (5-11), the third harmonic voltage of the heater is independent of the resistances R_3 and R_2 due to the fact that almost the whole current is passing through the other leg. However, measuring voltages of R_2 and R_3 can be used as a quick check for certifying the accuracy of the measurements. Below are these relations:

$$V_{R_1} + V_{R_A} \cong V_{R_2} \qquad 5\text{-}12$$

$$V_{R_s} \cong V_{R_3} \qquad 5\text{-}13$$

- **Measurement Tools**

Keithley series 2400 is a digital instrument which is being used both as power source and multimeter. It can produce power up to 20 (W) in voltage range from ±5μV (sourcing) and ±1μV (measuring) to ±200V DC and current from ±10pA to ±1A [28]. This instrument together with some ordinary multimeters is being used for voltage and current measurements in this work.

5.1.2. EXPERIMENTAL PROCEDURE STEPS

In this part, it is aimed at going through all steps to perform properly 3ω measurement. First of all, the measurement circuit needs to be setup according to following figure.

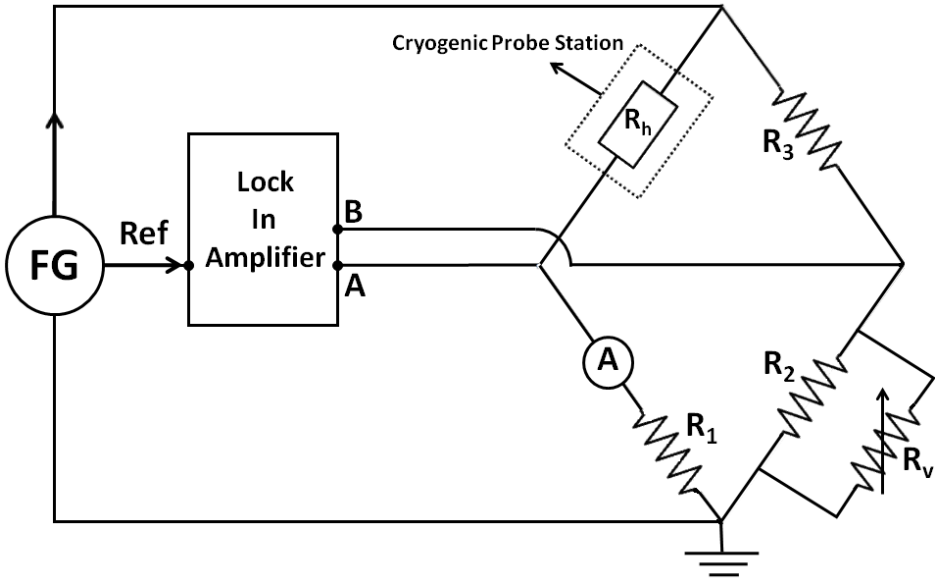

FIGURE 5-3: SCHEMATIC FIGURE OF MEASUREMENT CIRCUIT

As it is observed in this scheme, the specimen is configured as an arm of Wheatstone bridge which was already explained. The function generator (FG) provides desired signals both for lock-in amplifier and for stimulating the circuit.

The detailed procedure is in this order:

- **Placing the Specimen inside Cryogenic Probe Station**

The specimen is directly placed on the mounting plate (referred to as a chunk). In order to provide a better thermal contact between specimen and the mounting plate, a lubricant called Krytox®, is used in between. Then the two-stage pumping system creates a vacuum down to $5x10^{-5}$ Torr. It normally takes around half an hour to reach this pressure level. The low pressure atmosphere around the heater reduces significantly the convection heat losses.

It should be noticed that the probes need to be kept in safe distance from the specimen during pumping down process to prevent any unwanted damage to the vulnerable gold line heaters on the surface. The probes move during the pressure decrease in the chamber.

- **Probing the Specimen**

At this step, a desired pad (heater), which has been previously checked under microscope, is selected for connecting to the measurement circuit as shown in figure (5-3). It can be done by probing the outer pads and connecting the probes outlet to the measurement circuit through BNC connectors. It is crucial to mention that probing should be done under microscope in order to avoid any over-sliding of probes tip on the pads.

- **Adjusting the Current by Function Generator**

A small voltage signal is applied from the function generator and corresponding current value on multimeter verifies a closed circuit. To do so, at first, a sinusoidal output is generated by the function generator and the frequency and voltage of input signal are adjusted to 1 kHz and 200 mV_{rms} respectively. In case of closed circuit, the digital multimeter shows a stable amount of current depending on the resistivity of the gold line. Otherwise, it is required to reexamine the circuit and all connections to find the problem. In most cases, the error is caused by a loose connection between the probe tips and the pads.

The next step is increasing the current passing through the heater by increasing the value of the input voltage of function generator. The current level is inherently dependent upon the substrate under study. If a substrate with low thermal conductivity is being used, the passing current value is experimentally adjusted in a range between 10 mA and 15 mA. In case of specimen with high thermal conductivity, the passing current needs to be set to about 30 mA or even more. This is due to generating sufficient amount of heat to give us measurable third harmonic voltage (proportional to the temperature oscillation at the heater).

- **Balancing the Wheatstone Bridge by Lock-in Amplifier**

As stated in previous section, the lock-in amplifier is used for measuring a very minute third harmonic AC signals. In order to perform 3ω measurement in a more precise manner, it is crucial to attenuate the first harmonic of the voltage signal at the upper limit of linear region frequency. In other words, it is required to initially calculate the upper limit of the frequency range as per equation (3-26) then, set the frequency of the input signal to this value. Afterward, try to balance the Wheatstone bridge by altering the variable resistance (parallel to the R_2 resistor) to get the least possible fundamental harmonic voltage when lock-in amplifier is set to A-B.

What it is meant by attenuation of the first harmonic voltage components is confined to the lowering of the overall resultant. It can be performed by attempting to decrease either one or both components (X, Y).

It is worth mentioning that finding the upper limit of the linear region frequency is dependent on being aware of thermal diffusivity of the specimen of interest. However, in case of unknown materials, which addressed earlier in chapter 3, we can estimate the upper limit of linear region frequency just by comparing with materials of known characteristics. For instance, in case of glass specimen, by assuming the heater half-width as 10 microns and thermal diffusivity equal to $3.4x10^{-7}$ ($m^2.s^{-1}$), the upper limit of linear region frequency can be calculated by equation (3-26) as 10 Hz. So, this value can be used also for other materials with the same range or lower thermal conductivity than that of glass specimen.

- **Commencing of 3ω Measurement**

The third harmonic voltage can be measured from this step on. Note that at this step it is not necessary to care about frequency limits of linear region as discussed earlier. We just aim to make measurement over a wide frequency range and plot resultant data for further analysis. Therefore, to commence measuring, input signal frequency is set to around 0.01 Hz. Then it can be manually increased up to some kHz. After data stabilization, X, Y, R and θ at each frequency are recorded.

It should be noted that appropriate time constant needs to be chosen according to the input frequency values (As discussed in previous section). For instance, first a few measurements require long time to be stabilized however for frequencies above 1 Hz, it just need at TC of one second to read the stable data.

- **Measuring Current and Voltage of the Required Elements**

This is the last but not least part of 3ω measurement. At this point, it is required to measure and record the passing current (I) and voltages across the resistors *Rs*, R_1, R_2, R_3 and R_A at the frequency of 1 kHz. These data are used for both a quick check of the accuracy of the measurements and also for converting the measured data obtained from Wheatstone bridge ($W_{3\omega}$) to the 3ω voltage of the heater as per equation (5-11).

5.2. TCR MEASUREMENT

There is a single procedure to attain the temperature coefficient of resistance of the heater. However, the apparatus being used for this purpose is either climate chamber or cryogenic probe station. Below is a detailed description of these two approaches.

5.2.1. CLIMATE CHAMBER

The resistance of the gold strip used as the heater is influenced by the temperature. Hence, when heating, the resistance of the heater changes; when the heat is transported to the underneath substrate the heater temperature decreases and so does its resistance. Therefore, it is needed to find the rate of temperature dependency of the gold resistance.

As it is observed in equation (3-10), this parameter is defined as β_h . It is possible to calibrate the line by recording both voltage across and current through gold strip over a temperature range and plot the resultant gold resistance at different temperatures. Then, the slope of the regression line indicates the $\frac{dR}{dT}$ parameter. In order to measure resistance at various temperatures, a climate chamber is being used as shown in following figure.

FIGURE 5-4: PICTURE OF CLIMATE CHAMBER WITH TWO MICRO-PROBES INSIDE

First step is placing the specimen of interest inside the climate chamber and probing it by two micro probes as shown in figure (5-4). Then, connect the cables to a power supplier (Keithley 2400) and adjusting the voltage and current to 0.1 V and 10 mA respectively. It is necessary to note that the passing current should be kept as lowest as possible to prevent any temperature increase caused by Joule heating. Moreover, in order to increase the measurement precision, just let the power supply to run right at the measurement times (about every 15 minutes in our case).

Now everything is ready for running the climate chamber and recording relevant voltage and current of the heater for every two degree centigrade, starting from 20 ($℃/min$) up to 50 ($℃/min$). The rate of temperature increase in chamber manual control is set to 0.5 ($℃/min$). Also the relative humidity is adjusted to current measured value (30-40%).

The output diagrams for different pads of used specimens can be found in appendix 1-3.

5.2.2. CRYOGENIC PROBE STATION

The procedure is quite same as the climate chamber. We only need two probes of four available ones to connect them to the power supply (Keithley 2400) after probing the specimen of interest.

There are some advantages of using Cryogenic probe station. First, the equilibrium time can be significantly reduced due to having a pretty smaller volume compared to climate chamber. Secondly, it enables us to take our measurements in vacuum condition which makes the results more reliable. Moreover, it is possible to work in a wide temperature range compared to restricted working temperature of the climate chamber.

CHAPTER 6

6. RESULT AND DISCUSSION

This chapter is divided into two sections. First, the 3ω measurement results for two different known specimens (Glass and Sialone®) with various ranges of thermal conductivities are separately scrutinized. These are just for evaluating the accuracy of implemented set up through comparing their results to their actual values.

The second part is about characterizing the thermal conductivity of PEDOT:PSS. Similarly, the 3ω measurement results for this specimen are also analyzed and at the end some comparisons are made with its previously reported values.

Necessary to note is that all samples are prepared according to previously mentioned procedure in chapter 4. The gold/chrome thicknesses for all studied specimens are in order of 1500 Å and 150 Å respectively.

Moreover, all measurements, including 3-omega and TCR measurements, are taken in vacuum condition[6] provided by Cryogenic probe station. However, the TCR measurements for glass and Sialone® substrates are taken inside the climate chamber.

6.1. VALIDATION OF THE 3-OMEGA MEASUREMENT RESULTS

Below are the 3ω measurement results for two known specimens. The first one is ordinary window glass with low thermal conductivity and the second one is Sialone® with relatively high thermal conductivity than that of the glass.

The procedure is selecting different patterns on single specimen. Then, for each pattern, the in-phase and out-of-phase temperature oscillation of the heater in terms of different input excitation frequencies are measured and depicted in a graph. Also, the temperature coefficient of resistance (TCR) for each measured pattern is determined separately (appendix 1-3). Finally, by plotting the overall third harmonic voltage amplitude (V_R) versus natural logarithm of excitation frequencies (Lnf) and finding the slope of linear section of this graph (S), one would be able to derive an average value for thermal conductivity of that specimen as per equation (3-22).

Meanwhile, data tables for all measured specimens can be found in appendix 5-8.

[6] considering a pressure of about $5x10^{-5}$ Torr

6.1.1. GLASS SPECIMEN

A simple window glass specimen of 3 mm thickness is employed here for measuring its thermal conductivity. For this purpose, a gold pattern with various heaters length and width is vacuum deposited onto this specimen. Then two of these patterns are selected to be separately inspected. Below is the picture of one sample heater on glass specimen.

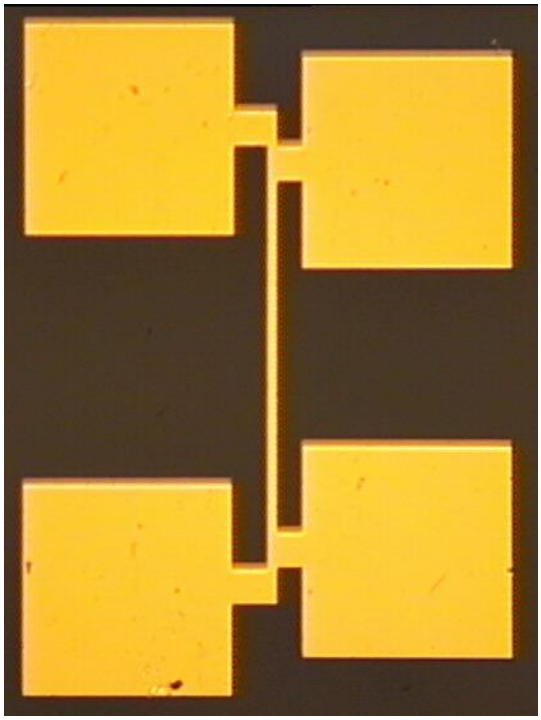

FIGURE 6-1: MICROSCOPIC PICTURE OF GOLD HEATER DEPOSITED ON GLASS SPECIMEN WITH 5X MAGNIFICATION

The table below describes the characteristics of these two patterns.

TABLE 2: CHARACTERISTICS OF TWO APPLIED PATTERNS IN CASE OF GLASS SPECIMEN

Pattern No.	Length (mm)	Width (µm)	V_h (mV)	I_h (mA)	R_h (Ω)	TCR (1/°K)
1	1.4	20	341	13.5	25.2	0.0024
2	3.4	50	350	13.5	25.9	0.0024

As it is observed in table 2, we have almost the same heater resistance for both patterns while the length and width are different. The reason is explained by equation 3-1, since there is a similar ratio between the length and cross-sectional area of the heater while assuming a homogenous thickness for both patterns.

The following graph shows the in-phase and out-of-phase components of temperature oscillations (ΔT_{AC}) versus thermal excitation frequencies (f) for the above mentioned patterns.

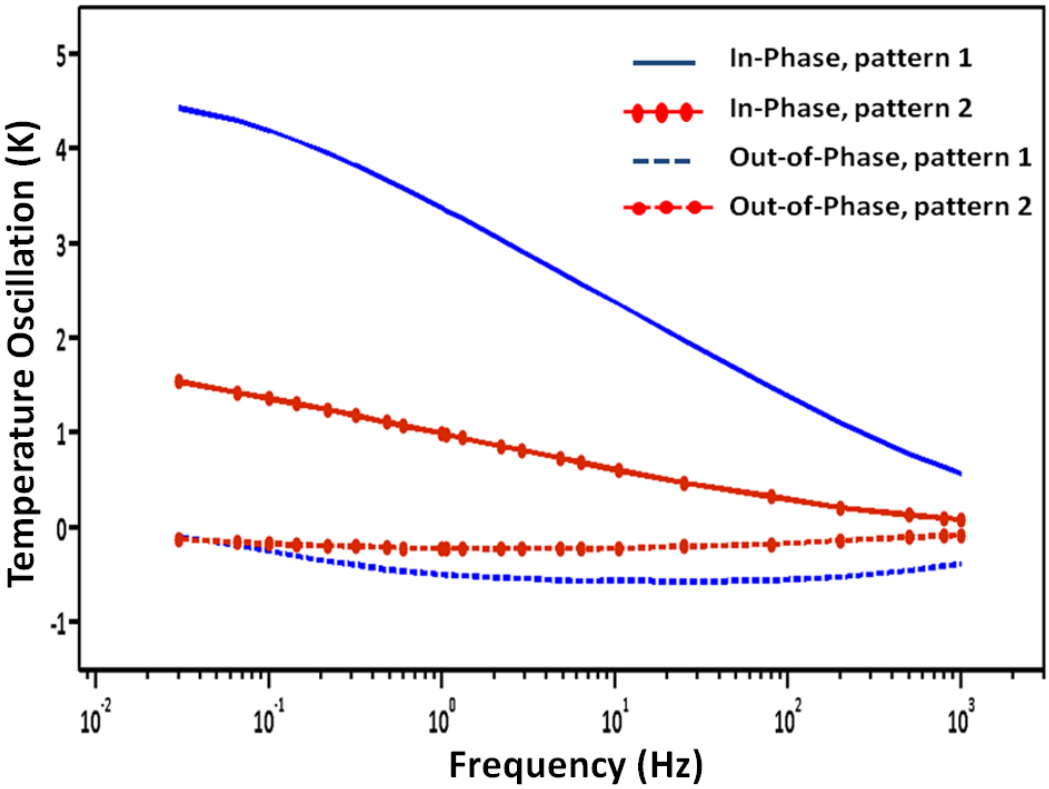

FIGURE 6-2: THE DIAGRAM OF THE IN-PHASE AND OUT-OF-PHASE COMPONENTS OF TEMPERATURE OSCILLATIONS (ΔT_{AC}) VERSUS THERMAL EXCITATION FREQUENCIES (F) FOR PATTERN1 (BLUE) AND PATTERN 2 (RED) IN CASE OF GLASS SPECIMEN

As it is clearly observed in graph (6-2), the in-phase component of temperature oscillation between the heater and underneath specimen for both patterns is reduced as the applied frequency is increased. The reason is obvious due to applying high frequency, the attributed penetration depth is low and it means that the heat affected region is confined to surface nearby. Therefore, there should not be much difference between heater temperature and this shallow depth. As it is seen the temperature oscillation approaches to zero by further increase of frequency. On the contrary, the opposite scenario is applied for low frequencies.

Another important difference between the two heaters is that the temperature oscillation for pattern number 1 (shorter one, blue color) is about three times greater that of the second one, despite the two patterns exhibit almost the same electrical resistivity. Therefore it can be concluded that the amount of heat losses for the pattern with larger surface area (Pattern 2) is higher than for the small pattern; which results in less temperature change between heater and the same penetration depth of the specimen as the first pattern. Therefore, the measurement result for patterns with larger surface area is less likely to be as accurate as the small ones.

As discussed earlier in chapter 3, in order to find the thermal conductivity of the specimen, it is required to plot the overall third harmonic voltage amplitude across the heater (V_R) versus natural logarithm of excitation frequencies (Lnf) for each pattern and try to find the slop of the linear region for each pattern. Here is the graph:

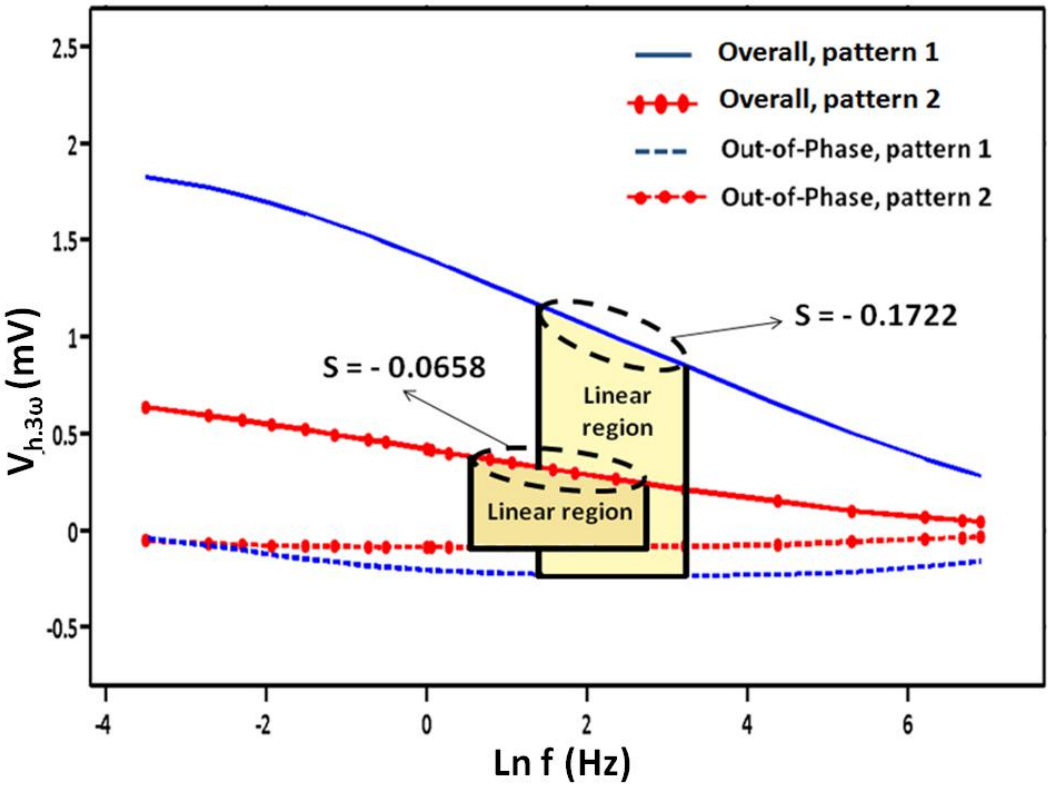

FIGURE 6-3: THE DIAGRAM OF THE OVERALL THIRD HARMONIC VOLTAGE AMPLITUDE ACROSS THE HEATER (V_R) VERSUS NATURAL LOGARITHM OF EXCITATION FREQUENCIES (LN F) FOR PATTERN 1 (BLUE) AND PATTERN 2 (RED), PARAMETER "S" INDICATES THE SLOPE OF THE LINEAR SECTION OF THE OVERALL THIRD HARMONIC VOLTAGE FOR EACH PATTERN

Now by considering equation (3-22) and substituting all required information listed in table 2 and parameter S, which comes from above graphs, the thermal conductivity of the glass can be derived as 1.26 and 1.39 ($W.m^{-1}.K^{-1}$) for first and second pattern respectively.

Although there is a wide range of discrepancy in reported results for thermal conductivity of the glass substrate [29,30], but about our case, the measurement results are in a good agreement with the values reported by Goodfellow Co., which is in a range between 1.2 ($W.m^{-1}.K^{-1}$) and 1.4 ($W.m^{-1}.K^{-1}$) in room temperature [31].

6.1.2. SIALONE® SPECIMEN

This special specimen was ordered from Goodfellow Co., a specialist supplier of metals, polymers which is originated in the UK. Sialone® is considered as ceramic material and it is composed of different components such as, silicon nitride, aluminum nitride, and aluminum oxide with unknown proportionality.

The picture below depicts one sample heater on Sialone® specimen.

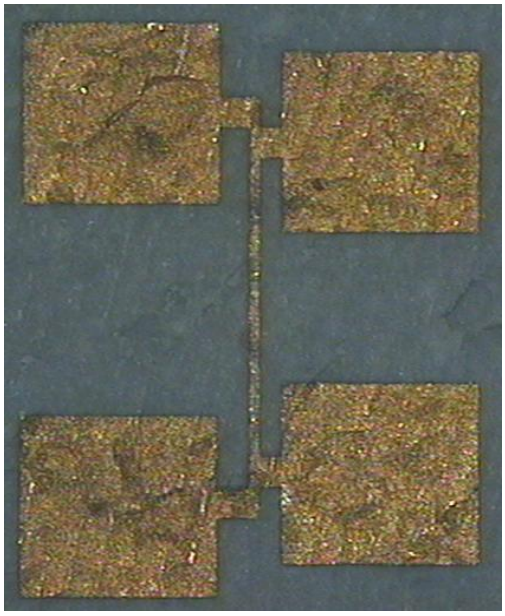

FIGURE 6-4: MICROSCOPIC PICTURE OF GOLD HEATER DEPOSITED ON SIALONE® SPECIMEN WITH 5X MAGNIFICATION

Unlike the glass substrate which was inspected in previous section, the surface of Sialone® is not flat enough for evaporating gold heater on top due to its morphological structure. The rough surface of the Sialone® specimen can easily be seen in figure 6-4. This surface fluctuation makes it hard to find gold heater patterns which are suitable for 3ω measurement. Therefore, we could only succeed to choose one appropriate pattern to be employed for this purpose. Table below describes the dimension and measurement characteristics of this pattern:

TABLE 3: CHARACTERISTICS OF THE APPLIED PATTERN IN CASE OF SIALONE® SPECIMEN

Length (mm)	Width (µm)	V_h (mV)	I_h (mA)	R_h (Ω)	TCR (1/°K)
1.4	30	1893	18.1	104.6	0.0017

According to above tabulated data, one can easily observe that the electrical resistivity for the specified pattern of Sialone® specimen is much higher than that of glass sample due to previously discussed rough surface. This high resistivity requires us to apply higher voltage for input signal to get the same amount of current and subsequent power as that of the glass sample for heating up the specimen.

The following graph depicts the in-phase and out-of-phase components of temperature oscillations (ΔT_{AC}) versus thermal excitation frequencies (f) for this single pattern. Here, a much higher frequency range is applied compared to glass specimen. However, the measurement results for very high frequencies are considered less reliable. In other words, by applying frequencies out of the scope of the linear region, we are actually involving with transition or planar region where more errors are expected to be included in measurement results.

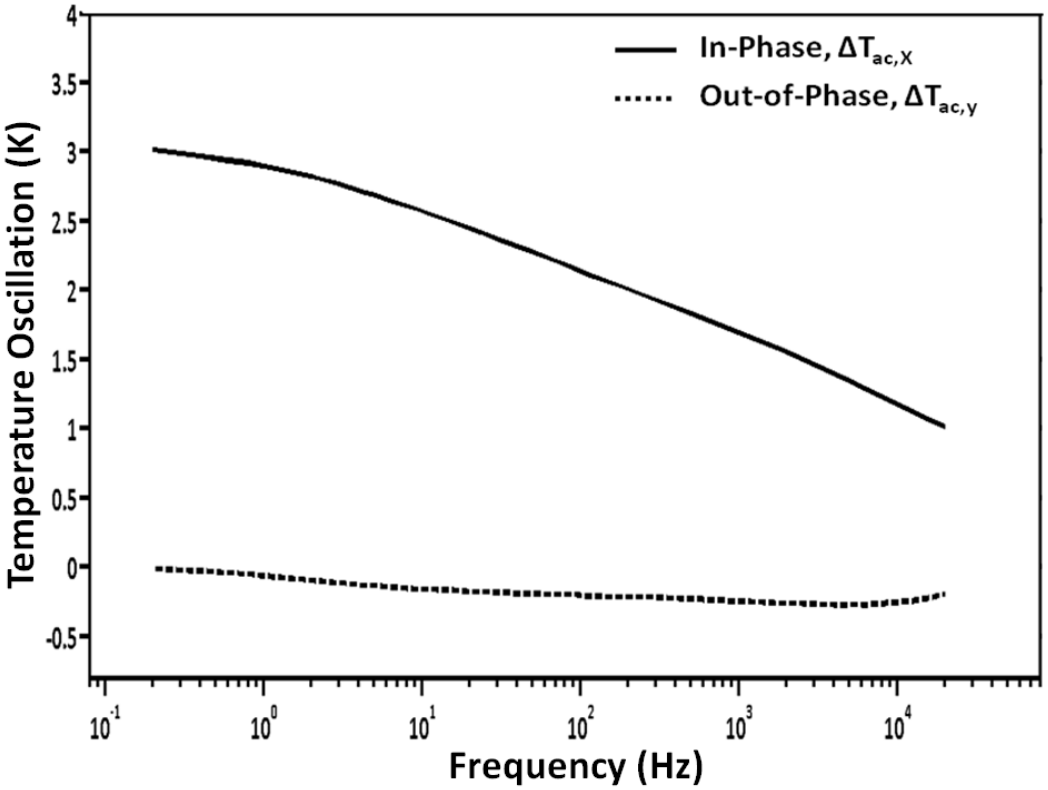

FIGURE 6-5: THE DIAGRAM OF THE IN-PHASE (SOLID LINE) AND OUT-OF-PHASE (DASHED LINE) COMPONENTS OF TEMPERATURE OSCILLATIONS (ΔT_{AC}) VERSUS THERMAL EXCITATION FREQUENCIES (F) FOR APPLIED PATTERN IN CASE OF SIALONE® SPECIMEN

As it is observed in figure (6-5), despite employing more power by the gold heater than that of glass sample but the temperature difference between the heater and the specimen is in a lower level compared to first pattern of the glass sample. It should be noted that the same length of patterns are being compared so the heat losses can be considered the same for both cases. The reason is due to the fact that Sialone® specimen is a much better thermal conductor than glass sample. Therefore, a great proportion of produced heat is conducted across the Sialone® specimen and it brings about less temperature difference between the heater and the underneath specimen.

Figure 6-6 depicts the overall third harmonic voltage amplitude across the heater (V_R) versus natural logarithm of excitation frequencies (Lnf) for specified pattern of Sialone® specimen. Moreover, the slope of the linear region is determined in the graph in order to be substituted in equation (3-22) along with other required data listed in table 4.

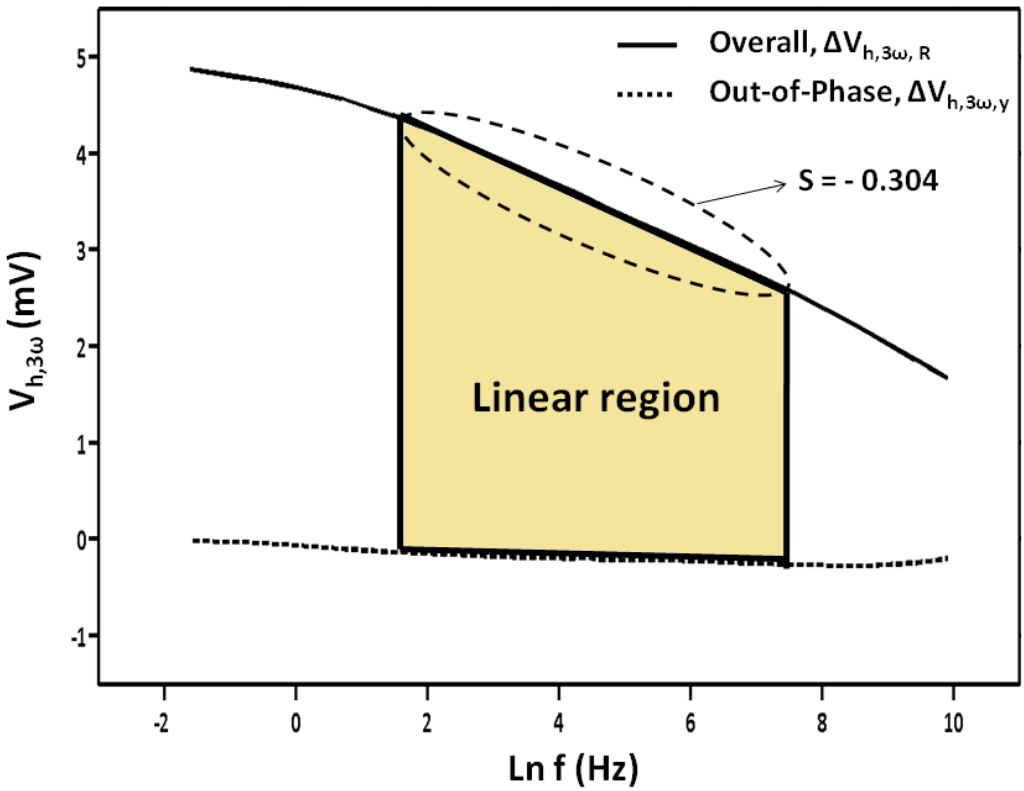

FIGURE 6-6: THE DIAGRAM OF THE OVERALL THIRD HARMONIC VOLTAGE AMPLITUDE ACROSS THE HEATER (V_R, SOLID LINE) VERSUS NATURAL LOGARITHM OF EXCITATION FREQUENCIES (LN F, DASHED LINE) FOR APPLIED PATTERN IN CASE OF SIALONE® SPECIMEN, PARAMETER "S" INDICATES THE SLOPE OF THE LINEAR SECTION OF THE OVERALL THIRD HARMONIC VOLTAGE.

As it is observed in above graph, the boundary range for frequency attributed to the linear region occurs in higher value than that of for glass sample. The reason is because of high thermal conductivity of Sialone® specimen which leads to higher level of frequency attributed to linear region. This is a proof of equation (3-26) which was already discussed in chapter 3.

Now the thermal conductivity of the Sialone® can be derived as 19.5 ($W.m^{-1}.K^{-1}$) which is considered a nice approximation of its real value reported by the producer as 20 ($W.m^{-1}.K^{-1}$) by considering an error of 2.5%.

6.2. THERMAL CONDUCTIVITY OF PEDOT:PSS

After validating the accuracy of the implemented set up, we can now proceed to the thermal characterization of PEDOT:PSS.

First of all, a half millimeter thick layer of PEDOT:PSS is made as already described in chapter 4. Then, prior to gold vapor deposition process, a 65 µm thick layer of Kapton® tape is applied to cover the surface. It is crucial to use this insulating layer between the gold heater and the substrate because PEDOT:PSS is electrically conducting. Hence if it is not properly electrically

insulated, the AC current signal would leak from the heater into the PEDOT:PSS and affect the result of the measurement.

Below is the picture of one sample heater on PEDOT:PSS specimen with a 65 µm thick layer of Kapton® tape on top.

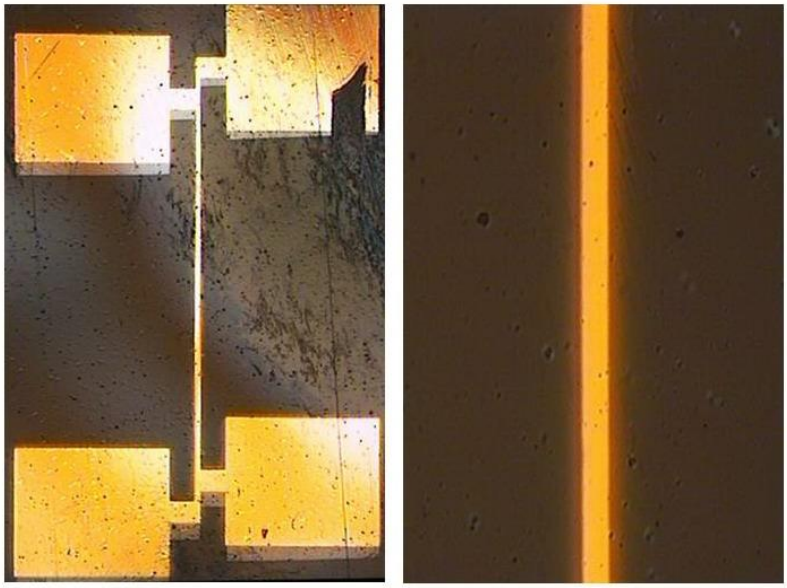

FIGURE 6-7: MICROSCOPIC PICTURE OF GOLD HEATER WITH MAGNIFICATION OF 5X ON TOP OF PEDOT:PSS COVERED BY KAPTON® TAPE (A) AND A SMALL PORTION OF GOLD LINE HEATER WITH 20X MAGNIFICATION (B)

As it is observed in figure (6-7-a), there are some shadow effects (gray color) beside the gold pattern which is actually a minor shift between gold and chrome layer. The reason as discussed earlier in chapter 4, is due to misalignment of shadow mask inside the Balzers BA510 evaporator. However it does not have any effect on the measurement results.

The next steps are the same as what done for glass and Sialone® specimens. In this case, two gold patterns are also selected with attributes listed in table below:

TABLE 4: CHARACTERISTICS OF TWO APPLIED PATTERNS IN CASE OF PEDOT:PSS SPECIMEN

Pattern No.	Length (mm)	Width (µm)	V_h (mV)	I_h (mA)	R_h (Ω)	TCR (1/°K)
1	2.15	20	395	12	32.9	0.0015
2	3.1	20	404	11	36.7	0.0020

The following graph depicts the in-phase and out-of-phase components of temperature oscillations (ΔT_{AC}) versus thermal excitation frequencies (f) for these two patterns. Interesting to

note is the high level of temperature difference between the heater and the specimen when it is compared with glass and Sialone® substrates. The reason is due to poor thermal conductivity of PEDOT:PSS, leading to temperature increase of heater itself rather than heat to be conducted through the underneath specimen.

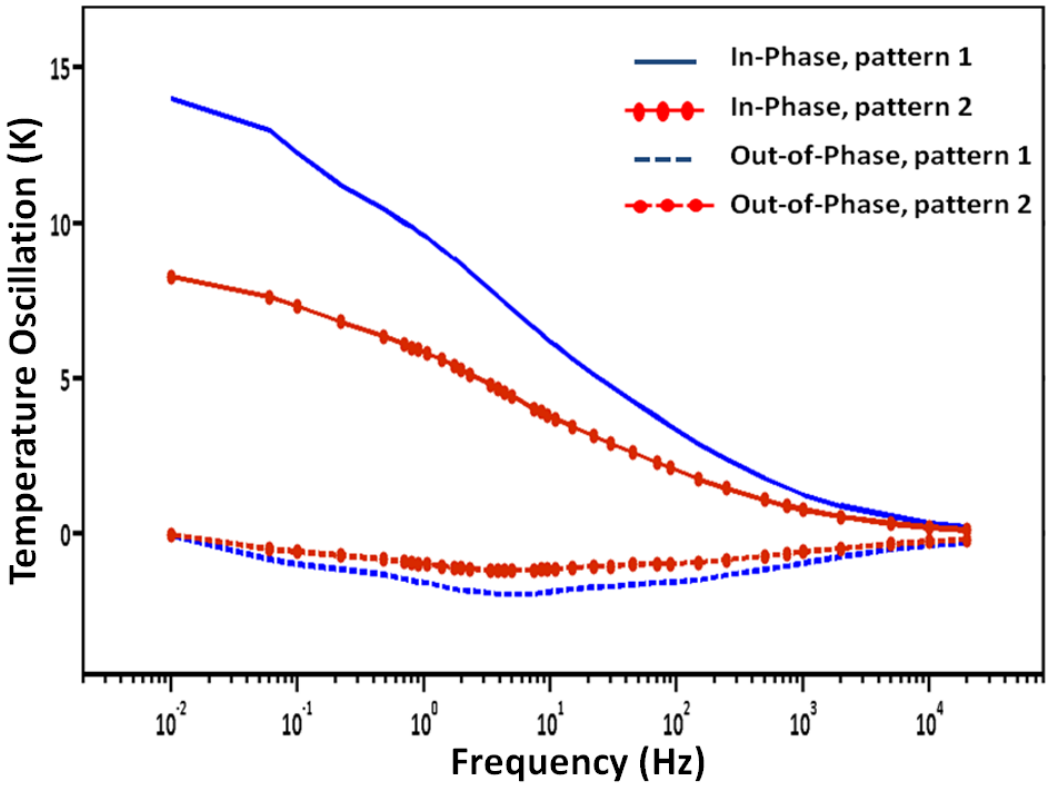

FIGURE 6-8: THE DIAGRAM OF THE IN-PHASE AND OUT-OF-PHASE COMPONENTS OF TEMPERATURE OSCILLATIONS (ΔT_{AC}) VERSUS THERMAL EXCITATION FREQUENCIES (F) FOR PATTERN1 (BLUE) AND PATTERN 2 (RED) IN CASE OF PEDOT:PSS SPECIMEN

It is necessary to mention that the applied frequency require to be small enough to pass through the isolating Kapton® tape and diffuse into the PEDOT:PSS layer. In order to distinguish how depth the generated heat is penetrated in underneath specimen, one can use equation (3-21) by assuming the thermal diffusion of 0.01 ($cm^2.s^{-1}$) for insulating Kapton® tape layer [27]. The border-line frequency between PEDOT:PSS layer and Kapton® tape is defined as follows:

$$f = \frac{D_K}{4\pi t_K^2} = \frac{10^{-2} \times 10^{-4}}{4\pi(65 \times 10^{-6})^2} \cong 18.8\, Hz$$

Where t_K and D_K are the thickness and thermal diffusivity values of Kapton® tape layer respectively. As it is observed in figure (6-9), the linear region attributed to the PEDOT:PSS layer is chosen on the left side of the natural logarithm of the calculated border line frequency which is equal to 2.9 (Hz). In other words, the frequency range smaller than 18.8 (Hz) is just of our interest to specify the thermal characteristics of underneath PEDOT:PSS layer.

Therefore, one of the advantages of applying 3ω technique reveals especially in case of measuring low thermal conductivity materials. The reason as it is observed in figure (6-8), is due

to high temperature level of the heater which leads to radiation losses from the surface in other applied methods.

Following graph depicts the overall third harmonic voltage amplitude across the heater (V_R) versus natural logarithm of excitation frequencies (Lnf) for two specified pattern on PEDOT:PSS substrate.

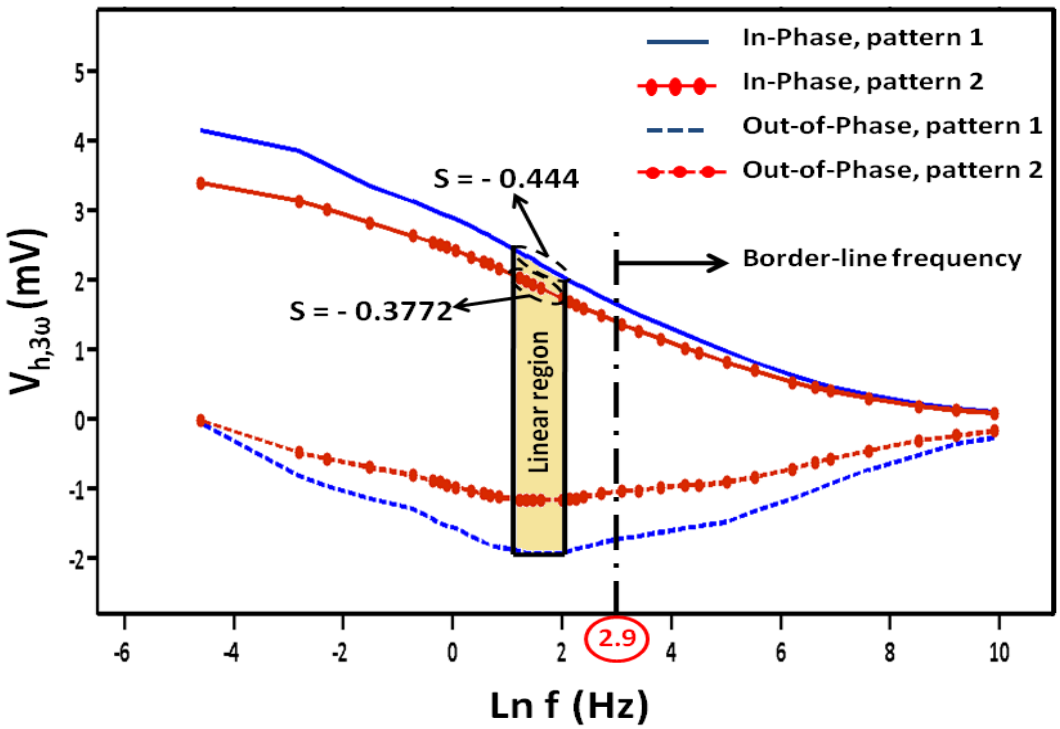

FIGURE 6-9: THE DIAGRAM OF THE OVERALL THIRD HARMONIC VOLTAGE AMPLITUDE ACROSS THE HEATER (V_R) VERSUS NATURAL LOGARITHM OF EXCITATION FREQUENCIES (LN F) FOR PATTERN 1 (BLUE) AND PATTERN 2 (RED), PARAMETER "S" INDICATES THE SLOPE OF THE LINEAR SECTION OF THE OVERALL THIRD HARMONIC VOLTAGE FOR EACH PATTERN

Similarly, the linear region is chosen in a way that the out-of-phase signals keep a constant value. In this case, the linear regions for both patterns overlap each other.

Now by considering equation (3-22) and substituting all required information listed in table 5 and parameter S, which comes from above graphs, the thermal conductivity of PEDOT:PSS can be achieved as 0.23 and 0.25 ($W.m^{-1}.K^{-1}$) for first and second patterns respectively.

The agreement between calculated and already measured thermal conductivity shows that measured data seems to be valid with a nice approximation [24].

6.3. THERMAL CONDUCTIVITY OF PEDOT:PSS AT DIFFERENT TEMPERATURES

The first pattern (table 5) was selected for determining the thermal conductivity variation of PEDOT:PSS substrate over a temperature range of 150 K. The reason for picking up the first pattern is its small surface area leading to less error compared to large patterns. Now, we start measuring the in-phase and out-of-phase components of temperature oscillations (ΔT_{AC}) versus thermal excitation frequencies (f) from 223 K up to 373 K. The measurements are performed in Cryogenic probe station to create desired temperatures. This measurement band is split into five different steps. Important to mention is that prior to making any measurement for these steps, an adequate time (about one hour) is spent to get as uniform temperature as possible within the vacuum chamber.

Following graph depicts all in-phase and out-of-phase components of temperature oscillations (ΔT_{AC}) versus thermal excitation frequencies (f) for the specified pattern over this temperature range.

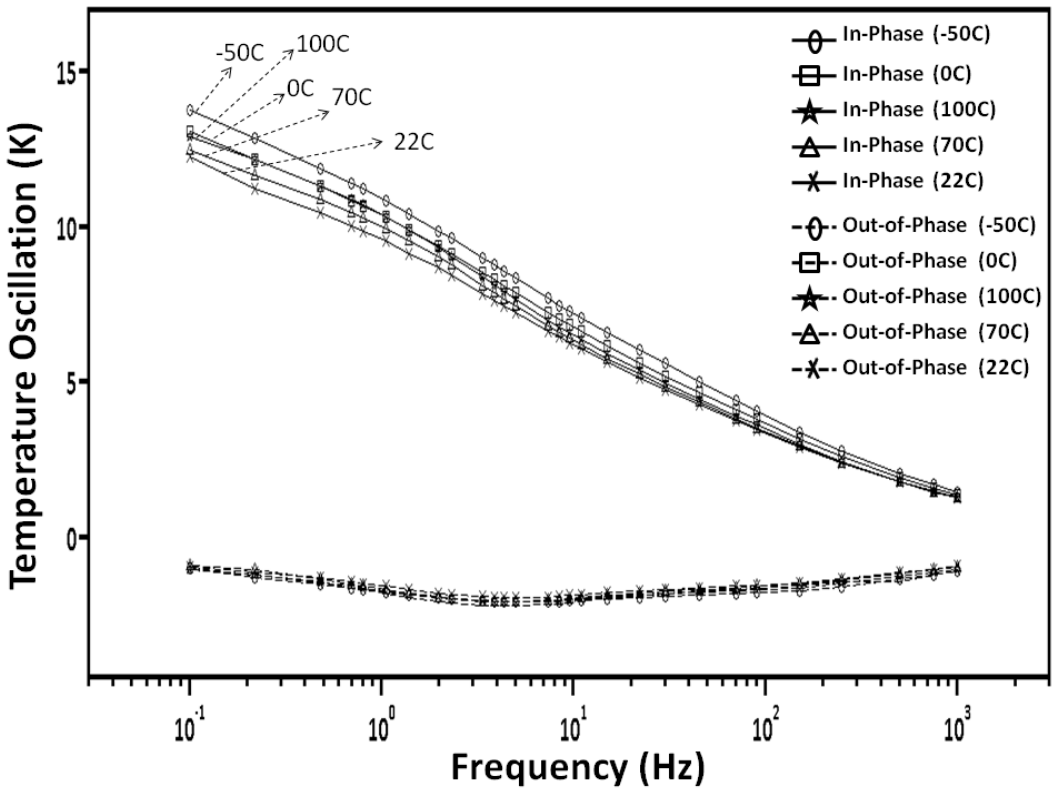

FIGURE 6-10: IN-PHASE (SOLID LINE) AND OUT-OF-PHASE (DASHED LINE) COMPONENTS OF TEMPERATURE OSCILLATIONS (ΔT_{AC}) VERSUS THERMAL EXCITATION FREQUENCIES (F) FOR DIFFERENT TEMPERATURES.

As it is observed in figure (6-10), the out of phase components of all temperature steps follow almost the same trend. However, in case of in-phase components of temperature oscillation, there are some differences especially at low frequencies.

It should be noted that all above depicted data is by assuming the $\frac{dR}{dT}$ value equal to 0.0495. However, the measured pattern exhibit slightly different behavior over new temperature band (223 K -373 K) in comparison with earlier $\frac{dR}{dT}$ measurement which was confined to a more limited scope (295 K- 315 K). It seems the new $\frac{dR}{dT}$ value would be more reliable because of covering a much broader range of temperature.

Below is the diagram of resistance change versus temperature change for the specified pattern under measurement.

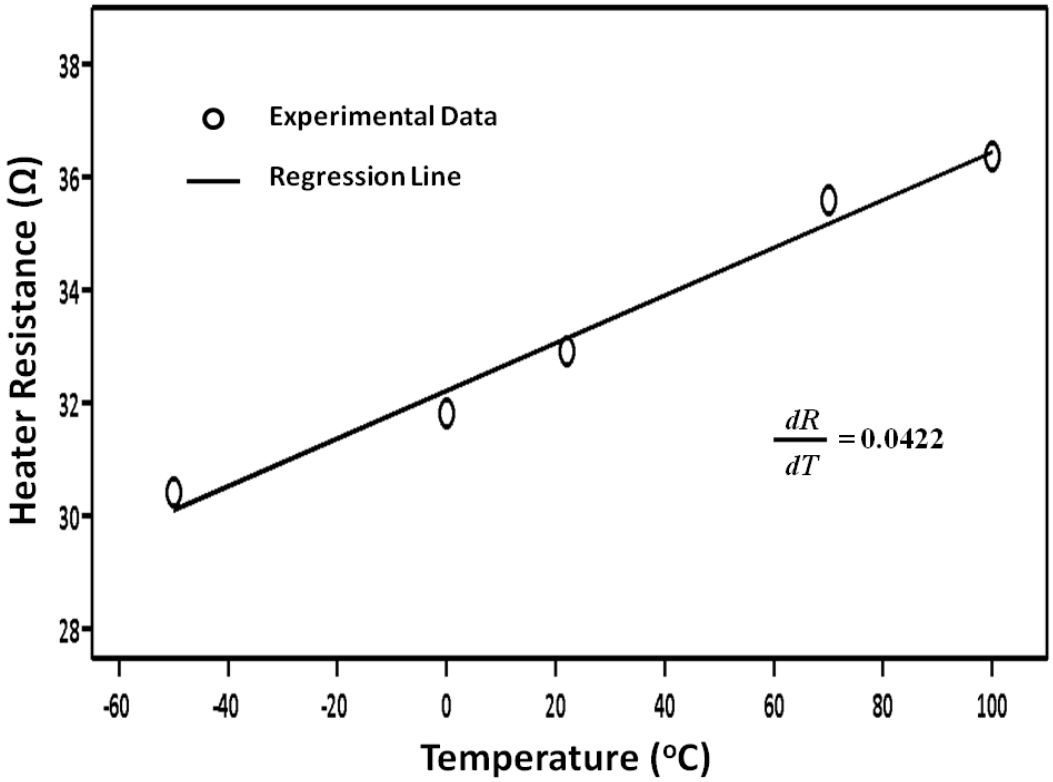

FIGURE 6-11: HEATER RESISTANCE CHANGE VERSUS TEMPERATURE CHANGE FOR THE FIRST PATTERN (MODIFIED TCR VALUE)

According to figure (6-11), a modified value can be obtained for $\frac{dR}{dT}$ which leads to a new TCR value equal to 0.0013 K^{-1} at room temperature.[7]

Table 5 describes all relevant data attributed to these temperature steps for both TCR values in order to illustrate the importance of this parameter in final thermal conductivity results. Parameter *S* is the slope of the linear section of the overall third harmonic voltage for each pattern. It should be noted that this parameter (S) is independent of TCR value so it does not change with modifying the TCR value.

[7] By assuming heater resistance equal to 32.9 (Ω) at room temperature

What is meant by original is assuming the previously calculated $\frac{dR}{dT}$ for a limited temperature range and modified is applied for values which have used the latest value of $\frac{dR}{dT}$ over a wider temperature range. This was just for clarifying the concept behind these expressions.

TABLE 5: MEASUREMENT DATA FOR DIFFERENT TEMPERATURES IN TERMS OF ORIGINAL (DR/DT=0.0495) AND MODIFIED (DR/DT=0.0422) VALUES

Temp (K)	V_h (mV)	R_h (Ω)	S	TCR (1/°K)		K (W.m^{-1}.K^{-1})	
				Original	Modified	Original	Modified
223	359	30.4	0.4723	0.0016	0.0014	0.19	0.17
273	382	31.8	0.4713	0.0016	0.0013	0.21	0.18
295	395	32.9	0.4440	0.0015	0.0013	0.23	0.20
343	427	35.6	0.4933	0.0014	0.0012	0.23	0.19
373	440	36.4	0.5400	0.0014	0.0012	0.22	0.19

Figure 6-12 clearly depicts the thermal conductivity change of PEDOT:PSS versus temperature change in terms of both original and modified TCR values.

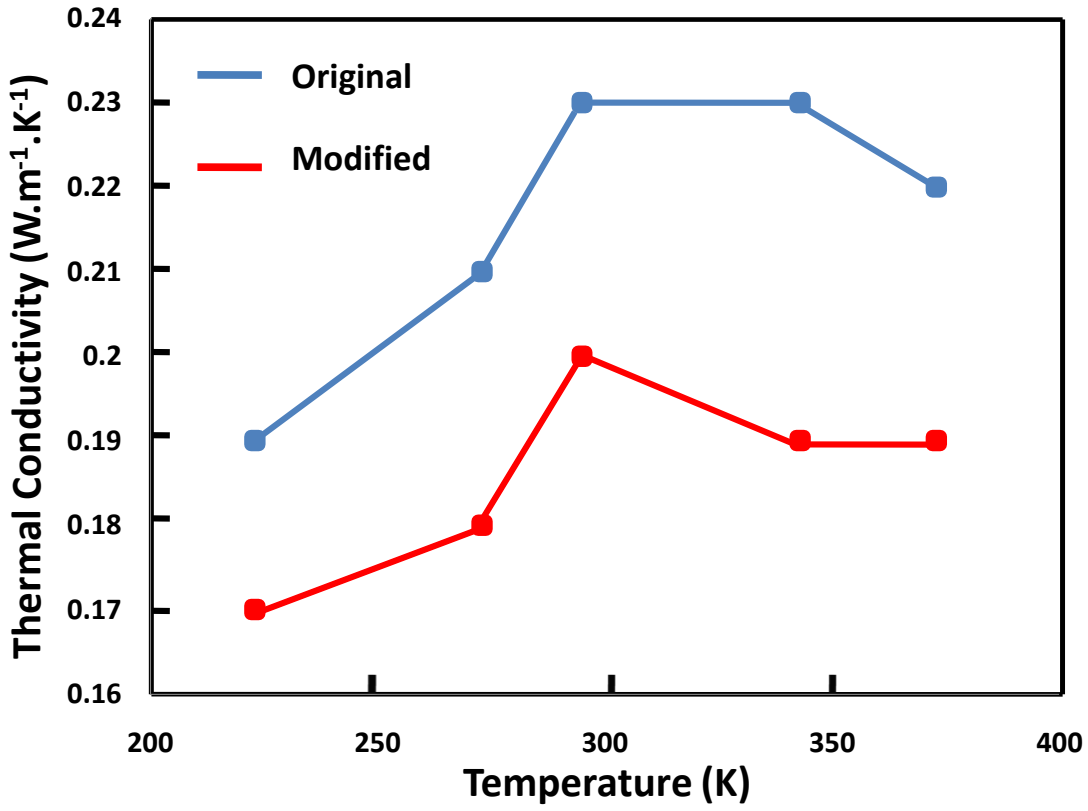

FIGURE 6-12: THERMAL CONDUCTIVITY CHANGE OF PEDOT:PSS VERSUS TEMPERATURE CHANGE IN TERMS OF BOTH ORIGINAL AND MODIFIED TCR VALUES

As it is observed in figure (6-12), the thermal conductivity is temperature dependent. The reason is explained by phonon scattering [12]. This phenomenon plays an important role in heat transfer in solids. Temperature gradient is considered an effective factor to stimulate phonons to scatter. The temperature dependence of phonon scattering is defined by Wien's displacement law. It states that there is a reverse proportionality between the wavelength distribution peaks at a value and temperature. In other words, it describes that the more the temperature increase, the more the phonon wavelength is decreased and vice versa. Therefore, by varying temperature, different scenarios for phonon scattering are dominated.

On this basis, at low temperatures, the phonon wavelength is long; so the boundary scattering is dominant. By increasing temperature, the phonon wavelength decreases and it approaches to defects. So, in room temperature range the most important factor is defect scattering. Finally, for higher temperatures, the wavelength is continuing to decrease and on the contrary wave vector increases. At that time, umklapp scattering became important. This phenomenon is the dominant process for thermal resistivity at high temperatures.

Meanwhile, as it is observed in figure (6-12), there is a considerable gap between the modified and original thermal conductivities of PEDOT:PSS. Therefore, it can be concluded that there is a strong dependency between the final result for thermal conductivity of a specimen and the accurate measurement of TCR value.

As discussed earlier in chapter 2.2, the dimensionless figure of merit (ZT) is a benchmark to determine how effective a material is for being used in thermo electric applications.
According to literature, there is a reverse relationship between the Seebeck coefficient (S) and electrical conductivity (σ) of PEDOT:PSS. In other words, the electrical conductivity of PEDOT:PSS can be enhanced by several orders of magnitude by altering PSS dopant concentration and also adding some dielectric solvents like dimethyl sulfoxide (DMSO). On the other hand, it causes significant decrease in Seebeck coefficient even with a small amount of DMSO. However, the maximum power factor is more attributed to electrical conductivity than Seebeck coefficient.
In our case, the employed PEDOT:PSS does not contain any additives. By browsing the literature, one finds an average power factor (σS^2) value equals to 4.42 ($\mu W.m^{-1}.K^{-2}$) while assuming the molar ratio of 1:2.5 [16].
Therefore, by substituting required values in equation (2-6), the ZT value at ambient temperature can be concluded as follows:

$$Z_T = \frac{(4.42)}{(0.2) \times (10^6)} \times (295) \cong 0.0065$$

In our case, the highest ZT value occurs at the temperature of 373K which is equal to 0.0087. However, it is still not comparable to reported dimensionless figure-of-merit values for inorganic semiconductors which are about 0.9 as a consequence of poor power factor. So, it demands lots of research and study towards improving the electrical characteristics of the organic polymers.

CHAPTER 7

7. CONCLUSION AND PERSPECTIVES

7.1. CONCLUSION

In this diploma work, we aim at measuring the thermal conductivity of a novel organic conducting polymer. The method employed to fulfill this target was the 3ω technique. The first step was to validate the accuracy of implemented set up by using glass and Sialone® specimens with known thermal characteristics as benchmarks. For glass specimen, the average thermal conductivity result was 1.3 ($W.m^{-1}.K^{-1}$) which is exactly in the range reported by Goodfellow Co. About the Sialone® substrate, the measured thermal conductivity was 19.5 ($W.m^{-1}.K^{-1}$) which is also in a nice agreement with its actual value by considering an error of 2.5%.

Therefore, we concluded that the measurement set up is working properly providing an acceptable error.

Before proceeding to thermally characterize the PEDOT:PSS, it was required to make a thick layer of this polymer. For this purpose, about half a millimeter thick layer of this material was successfully made by applying a PDMS mould. This was an innovative way of creating PEDOT:PSS layer ever made with such a thickness.

Then, two different patterns with various dimensions (length and width) were selected to be studied separately. The average result of both patterns was 0.24 ($W.m^{-1}.K^{-1}$), while the only value reported in the literature is 0.17 ($W.m^{-1}.K^{-1}$) at room temperature [12]. This amount of error was a bit suspicious and it was deduced that some input data are likely to be the source of errors, more especially the temperature coefficient of resistance (TCR) of the heater. After correction, at the same time, the gold resistance change over this temperature range was studied and a modified value could be obtained for temperature coefficient of resistance (TCR) of the heater. The latest value was applied again to modify the thermal conductivity of the first pattern. It is worth mentioning that the previous TCR value was obtained in a limited range of temperatures as that of the modified one. The result showed a considerable improvement in thermal conductivity from 0.23 (W.m-1.K-1) to 0.20 (W.m-1.K-1) at room temperature. By this amendment the amount of errors could be halved. It clearly shows the crucial role of specifying as precise value as possible for temperature coefficient of resistance of the heater.

After corrections, the thermal conductivity of PEDOT:PSS was measured at different temperatures ranging from 223 K to 373 K. It showed an increase in thermal conductivity as the temperature went up from 223 K to ambient temperature and then started to decline by further increasing the temperature. Finally, it saturated and followed a constant trend over temperature range above 343 K. It varies between 0.17-0.2 ($W.m^{-1}.K^{-1}$) which the minimum measured

thermal conductivity belongs to starting point of the measurement (223 K) and the highest value, as mentioned earlier, occurs in room temperature (295 K).

To sum up, in order to enhance the accuracy of the 3ω technique, two important points needs to be especially taken into consideration. First is using as short as possible gold pattern for creating heat over the specimen. This point particularly emerges in case of substrates with very low thermal conductivities. The other crucial point, as discussed above is finding the most reliable approach for determination of TCR value of the heater with the least possible error while even a minor amount of error would be of a great impact on the final results.

7.2. PERSPECTIVES

According to above mentioned results, it is possible to draw horizons for the future works to provide answers to some fundamental questions as for measuring the thermal conductivity by 3ω method.

First of all, it is needed to find the optimum value for the surface area of the heater in order to have the least possible errors caused by heat losses through conduction, convection and radiation to the air. What is meant by optimum value is finding the shortest value for heater length and width provided a sufficient amount of heat could be produced in heater.

The other area which needs to be addressed is exploring alternative approaches for TCR measurement of the heater to prevent reporting of any incorrect value for thermal conductivity.

Moreover, there should be some research to make 3ω measurement technique compatible with materials in states other than solid. It can be done by altering geometries of heater on the specimen.

Meanwhile, lots of research and study needs to be done to enhance the power factor of organic polymers to a value comparable to that of inorganic ones.

APPENDIX

1- Heater resistance change versus temperature change for the patterns 1 and 2 on glass substrate

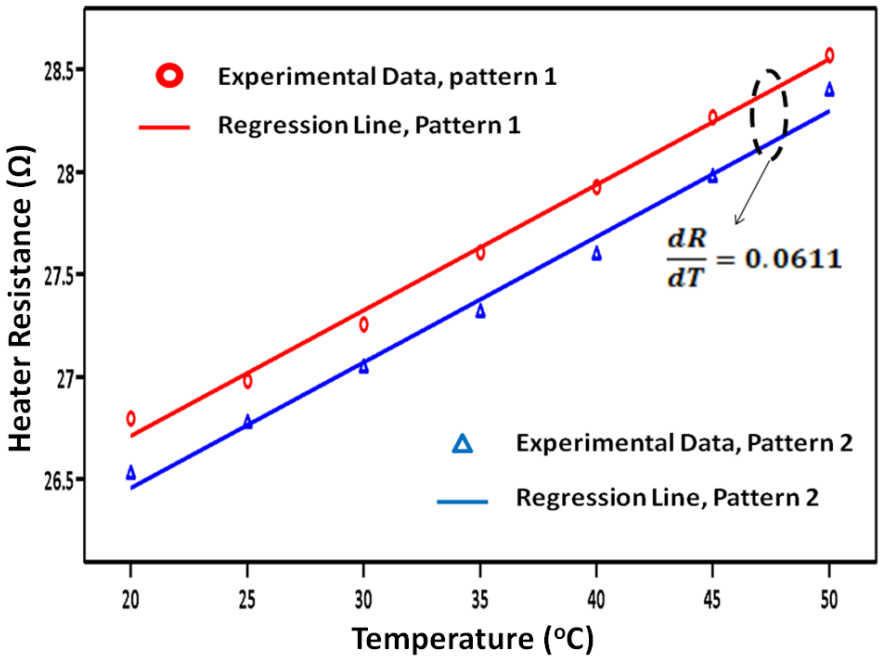

2- Heater resistance change versus temperature change for the pattern on Sialone® substrate

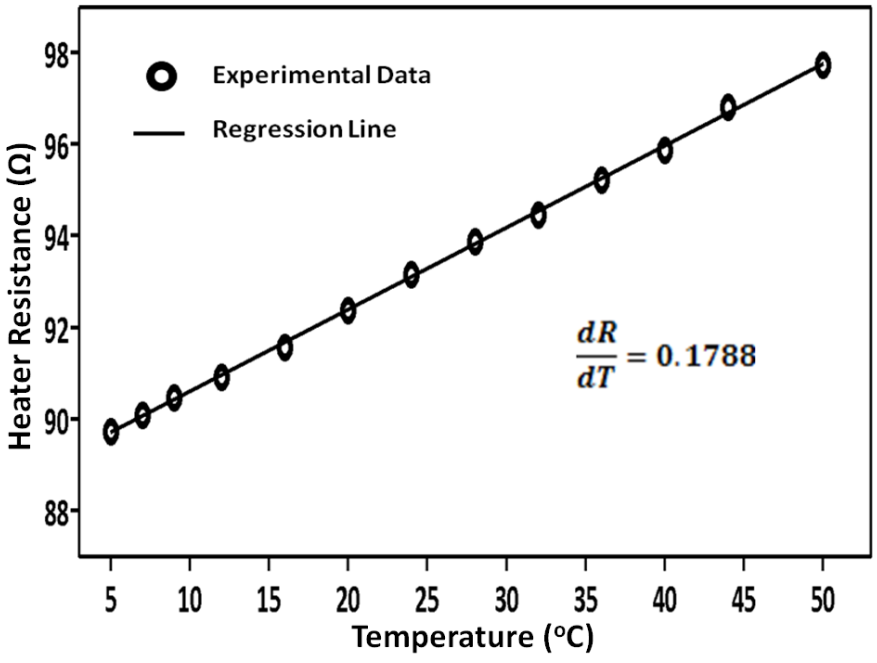

3- Heater resistance change versus temperature change for the patterns 1 and 2 on PEDOT:PSS

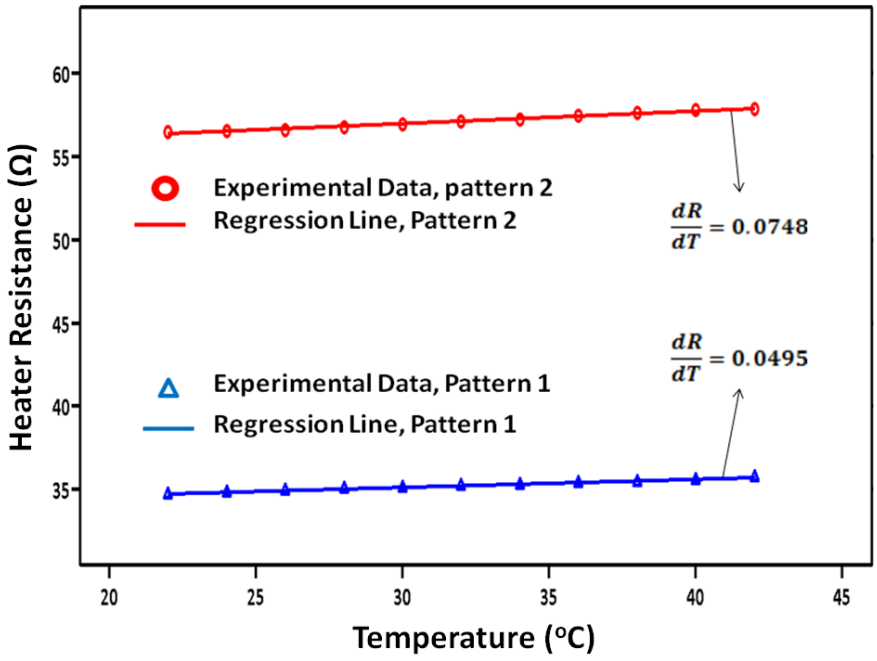

4- The diagram of the overall third harmonic voltage amplitude across the heater (V_R) versus natural logarithm of excitation frequencies (Ln f) for pattern 1 on the PEDOT:PSS specimen in terms of different temperatures. Dashed lines indicate the out of phase component of the third harmonic voltage for different temperatures.

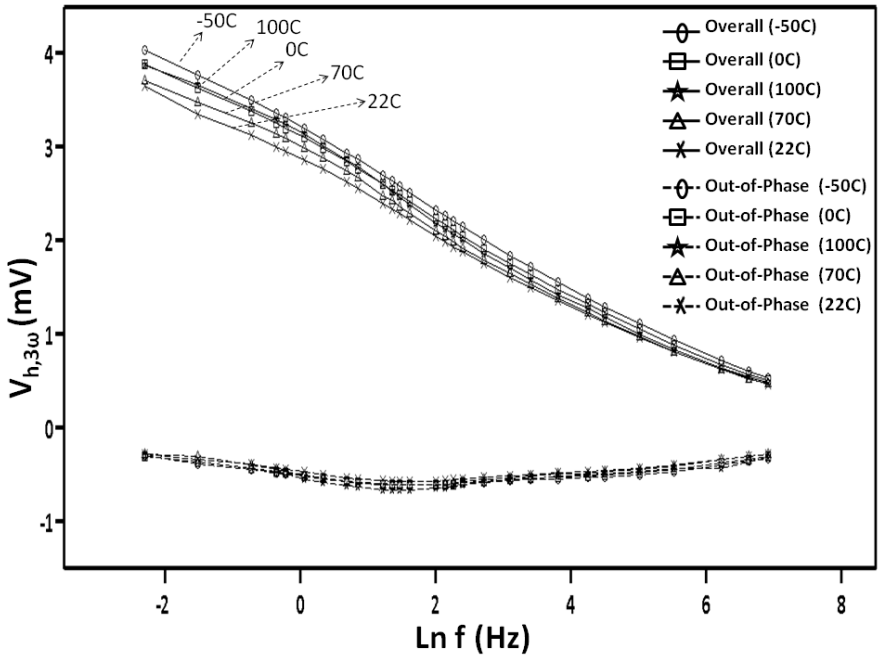

5- Data table containing all detailed measurement data for Sialone® specimen

f(Hz)	V_y(mV)	V_R(mV)	ΔT_x (K)	ΔT_y (K)
0.20	-0.0206	4.8691	3.0155	-0.0128
0.40	-0.0413	4.7969	2.9708	-0.0255
0.60	-0.0619	4.7556	2.9390	-0.0383
0.80	-0.0825	4.7144	2.9198	-0.0510
1.00	-0.1032	4.6834	2.8943	-0.0638
2.00	-0.1547	4.5700	2.8242	-0.0956
2.19	-0.1651	4.5493	2.8115	-0.1020
3.00	-0.1857	4.4771	2.7668	-0.1148
4.38	-0.2166	4.3946	2.7095	-0.1339
4.82	-0.2166	4.3636	2.6967	-0.1339
6.57	-0.2373	4.2811	2.6457	-0.1466
9.63	-0.2579	4.1780	2.5819	-0.1594
10.56	-0.2579	4.1470	2.5628	-0.1594
14.45	-0.2682	4.0645	2.5054	-0.1658
21.13	-0.2888	3.9510	2.4353	-0.1785
23.19	-0.2888	3.9201	2.4226	-0.1785
30.69	-0.2992	3.8375	2.3652	-0.1849
46.38	-0.3095	3.7137	2.2887	-0.1913
69.57	-0.3198	3.5899	2.2122	-0.1976
90.00	-0.3198	3.5074	2.1612	-0.1976
110.00	-0.3404	3.4455	2.1166	-0.2104
180.00	-0.3507	3.2908	2.0273	-0.2168
250.00	-0.3507	3.1979	1.9636	-0.2168
500.00	-0.3714	2.9813	1.8297	-0.2295
1000.00	-0.4023	2.7647	1.6958	-0.2486
2000.00	-0.4230	2.5480	1.5555	-0.2614
5000.00	-0.4436	2.2179	1.3452	-0.2741
6000.00	-0.4436	2.1457	1.3005	-0.2741
12000.00	-0.4023	1.8672	1.1284	-0.2486
15000.00	-0.3714	1.7847	1.0774	-0.2295
20000.00	-0.3198	1.6712	1.0137	-0.1976

6- Data table containing all detailed measurement data for Glass specimen

f(Hz)	Pattern No. 1				Pattern No. 2			
	V_y(mV)	V_R(mV)	ΔT_x (K)	ΔT_y (K)	V_y(mV)	V_R(mV)	ΔT_x (K)	ΔT_y (K)
0.03	-0.0397	1.8264	4.4252	-0.0962	-0.0506	0.6364	1.5420	-0.1225
0.07	-0.0794	1.7714	4.2920	-0.1924	-0.0654	0.5918	1.4267	-0.1585
0.10	-0.1008	1.7317	4.1884	-0.2442	-0.0714	0.5680	1.3619	-0.1729
0.14	-0.1252	1.6890	4.0848	-0.3034	-0.0773	0.5442	1.3042	-0.1873
0.22	-0.1466	1.6371	3.9516	-0.3552	-0.0803	0.5205	1.2466	-0.1946
0.32	-0.1619	1.5851	3.8184	-0.3922	-0.0833	0.4937	1.1817	-0.2018
0.48	-0.1833	1.5240	3.6630	-0.4440	-0.0862	0.4669	1.1097	-0.2090
0.60	-0.1894	1.4874	3.5742	-0.4588	-0.0892	0.4550	1.0736	-0.2162
1.00	-0.2046	1.4049	3.3670	-0.4958	-0.0892	0.4193	0.9944	-0.2162
1.06	-0.2077	1.3958	3.3448	-0.5032	-0.0892	0.4134	0.9800	-0.2162
1.31	-0.2107	1.3591	3.2560	-0.5106	-0.0892	0.3985	0.9439	-0.2162
2.19	-0.2199	1.2705	3.0340	-0.5328	-0.0922	0.3658	0.8575	-0.2234
2.89	-0.2230	1.2217	2.9082	-0.5402	-0.0922	0.3480	0.8142	-0.2234
4.82	-0.2291	1.1331	2.6862	-0.5550	-0.0922	0.3152	0.7350	-0.2234
6.34	-0.2321	1.0842	2.5678	-0.5624	-0.0922	0.2974	0.6845	-0.2234
10.56	-0.2291	0.9957	2.3532	-0.5550	-0.0892	0.2647	0.6053	-0.2162
25.00	-0.2352	0.8491	1.9758	-0.5698	-0.0833	0.2112	0.4684	-0.2018
80.00	-0.2291	0.6505	1.4800	-0.5550	-0.0744	0.1517	0.3243	-0.1801
200.00	-0.2168	0.5039	1.1026	-0.5254	-0.0565	0.1011	0.2090	-0.1369
500.00	-0.1863	0.3726	0.7770	-0.4514	-0.0416	0.0684	0.1297	-0.1009
800.00	-0.1680	0.3115	0.6364	-0.4070	-0.0357	0.0535	0.1009	-0.0865
1000.00	-0.1588	0.2840	0.5772	-0.3848	-0.0327	0.0476	0.0865	-0.0793

7- Data table containing all measurement data for PEDOT:PSS specimen

f(Hz)	Pattern No. 1				Pattern No. 2			
	V_y(mV)	V_R(mV)	ΔT_x (K)	ΔT_y (K)	V_y(mV)	V_R(mV)	ΔT_x (K)	ΔT_y (K)
0.01	-0.0179	4.1592	14.0039	-0.0604	-0.0098	3.4047	8.2760	-0.0239
0.06	-0.2420	3.8634	13.0079	-0.8149	-0.1968	3.1390	7.6301	-0.4784
0.10	-0.2868	3.6572	12.2534	-0.9658	-0.2362	3.0210	7.3192	-0.5741
0.22	-0.3406	3.3524	11.2273	-1.1469	-0.2854	2.8242	6.8408	-0.6936
0.48	-0.3854	3.1283	10.4426	-1.2978	-0.3346	2.6372	6.3624	-0.8132
0.70	-0.4303	3.0028	10.0200	-1.4487	-0.3641	2.5388	6.1233	-0.8850
0.80	-0.4482	2.9580	9.8691	-1.5090	-0.3739	2.5093	6.0037	-0.9089
0.90	-0.4571	2.9222	9.7182	-1.5392	-0.3936	2.4699	5.9319	-0.9568
1.06	-0.4661	2.8684	9.5371	-1.5694	-0.4035	2.4207	5.8123	-0.9807
1.39	-0.5020	2.7698	9.1448	-1.6901	-0.4231	2.3321	5.5970	-1.0285
1.75	-0.5289	2.6801	8.8430	-1.7807	-0.4428	2.2633	5.4057	-1.0764
1.97	-0.5378	2.6353	8.6921	-1.8109	-0.4527	2.2239	5.2861	-1.1003
2.32	-0.5468	2.5636	8.4205	-1.8410	-0.4625	2.1649	5.1426	-1.1242
3.37	-0.5647	2.4023	7.8470	-1.9014	-0.4822	2.0271	4.7838	-1.1720
3.85	-0.5737	2.3395	7.6358	-1.9316	-0.4822	1.9779	4.6881	-1.1720
4.33	-0.5737	2.2947	7.4547	-1.9316	-0.4822	1.9385	4.5446	-1.1720
5.00	-0.5737	2.2230	7.2434	-1.9316	-0.4822	1.8795	4.4250	-1.1720
7.39	-0.5737	2.0527	6.6398	-1.9316	-0.4822	1.7319	4.0423	-1.1720
8.45	-0.5647	1.9899	6.4587	-1.9014	-0.4723	1.6925	3.9466	-1.1481
9.51	-0.5558	1.9362	6.2474	-1.8712	-0.4723	1.6433	3.8270	-1.1481
10.95	-0.5468	1.8824	6.0663	-1.8410	-0.4625	1.5941	3.7074	-1.1242
15.00	-0.5289	1.7569	5.6438	-1.7807	-0.4428	1.4859	3.4443	-1.0764
22.00	-0.5109	1.6045	5.1307	-1.7203	-0.4231	1.3580	3.1573	-1.0285
30.00	-0.5020	1.4969	4.7686	-1.6901	-0.4231	1.2694	2.9181	-1.0285
45.00	-0.4840	1.3625	4.2857	-1.6298	-0.4035	1.1513	2.6311	-0.9807
70.00	-0.4661	1.2101	3.7726	-1.5694	-0.3936	1.0234	2.2962	-0.9568
90.00	-0.4571	1.1294	3.4708	-1.5392	-0.3936	0.9545	2.1288	-0.9568
150.00	-0.4392	0.9681	2.8974	-1.4789	-0.3739	0.8167	1.7700	-0.9089
250.00	-0.3944	0.8157	2.3843	-1.3280	-0.3444	0.6987	1.4830	-0.8372
500.00	-0.3406	0.6275	1.7807	-1.1469	-0.2952	0.5314	1.1003	-0.7176
750.00	-0.3048	0.5289	1.4789	-1.0261	-0.2558	0.4527	0.9089	-0.6219
1000.00	-0.2779	0.4661	1.2676	-0.9356	-0.2362	0.4035	0.7893	-0.5741
2000.00	-0.2151	0.3496	0.9054	-0.7243	-0.1870	0.2952	0.5501	-0.4545
5000.00	-0.1524	0.2151	0.5734	-0.5131	-0.1279	0.1870	0.3349	-0.3109
10000.00	-0.1076	0.1524	0.3622	-0.3622	-0.0984	0.1279	0.2153	-0.2392
20000.00	-0.0807	0.0986	0.2414	-0.2716	-0.0689	0.0886	0.1196	-0.1674

8- Data table containing all measurement data for PEDOT:PSS specimen over temperature range between 223-373 K

	f(Hz)	0.10	0.22	0.48	0.70	0.80	1.06	1.39	1.97	2.32	3.37	3.85	4.33	5.00	7.39
T=223 (K)	V_y(mV)	-0.30	-0.38	-0.45	-0.48	-0.50	-0.51	-0.55	-0.57	-0.58	-0.60	-0.61	-0.61	-0.61	-0.61
	V_R(mV)	4.04	3.77	3.50	3.37	3.32	3.20	3.09	2.93	2.87	2.70	2.64	2.58	2.51	2.33
	ΔT_x (K)	13.78	12.84	11.87	11.42	11.22	10.82	10.40	9.86	9.63	9.01	8.78	8.58	8.35	7.70
	ΔT_y (K)	-1.02	-1.31	-1.53	-1.65	-1.70	-1.76	-1.87	-1.96	-1.99	-2.05	-2.07	-2.07	-2.07	-2.07
T=273 (K)	V_y(mV)	-0.31	-0.36	-0.43	-0.47	-0.48	-0.51	-0.54	-0.57	-0.59	-0.61	-0.61	-0.61	-0.61	-0.61
	V_R(mV)	3.89	3.63	3.38	3.25	3.20	3.11	2.99	2.85	2.77	2.61	2.54	2.49	2.41	2.23
	ΔT_x (K)	13.06	12.15	11.31	10.84	10.67	10.32	9.91	9.38	9.12	8.54	8.31	8.10	7.87	7.23
	ΔT_y (K)	-1.05	-1.22	-1.46	-1.57	-1.63	-1.72	-1.81	-1.92	-1.98	-2.04	-2.07	-2.07	-2.07	-2.07
T=295 (K)	V_y(mV)	-0.29	-0.34	-0.39	-0.43	-0.45	-0.47	-0.50	-0.54	-0.55	-0.56	-0.57	-0.57	-0.57	-0.57
	V_R(mV)	3.66	3.35	3.13	3.00	2.96	2.87	2.77	2.64	2.56	2.40	2.34	2.29	2.22	2.05
	ΔT_x (K)	12.25	11.23	10.44	10.02	9.87	9.54	9.14	8.69	8.42	7.85	7.64	7.45	7.24	6.64
	ΔT_y (K)	-0.97	-1.15	-1.30	-1.45	-1.51	-1.57	-1.69	-1.81	-1.84	-1.90	-1.93	-1.93	-1.93	-1.93
T=343 (K)	V_y(mV)	-0.28	-0.31	-0.40	-0.45	-0.47	-0.51	-0.54	-0.57	-0.59	-0.61	-0.61	-0.61	-0.61	-0.60
	V_R(mV)	3.71	3.49	3.26	3.14	3.09	3.00	2.89	2.75	2.67	2.48	2.43	2.36	2.29	2.11
	ΔT_x (K)	12.48	11.67	10.90	10.48	10.28	9.96	9.57	9.03	8.77	8.09	7.90	7.67	7.45	6.80
	ΔT_y (K)	-0.93	-1.03	-1.35	-1.52	-1.58	-1.71	-1.81	-1.93	-2.00	-2.06	-2.06	-2.06	-2.06	-2.03
T=373 (K)	V_y(mV)	-0.30	-0.36	-0.43	-0.49	-0.50	-0.55	-0.58	-0.62	-0.63	-0.66	-0.66	-0.66	-0.66	-0.64
	V_R(mV)	3.88	3.67	3.41	3.29	3.25	3.14	3.01	2.87	2.79	2.60	2.52	2.47	2.39	2.19
	ΔT_x (K)	12.92	12.17	11.29	10.87	10.71	10.32	9.89	9.34	9.05	8.40	8.14	7.91	7.68	7.00
	ΔT_y (K)	-1.01	-1.20	-1.43	-1.63	-1.66	-1.82	-1.95	-2.08	-2.12	-2.21	-2.21	-2.21	-2.21	-2.15
	f(Hz)	8.45	9.51	10.95	15.00	22.00	30.00	45.00	70.00	90.00	150.00	250.00	500.00	750.00	1000.00
T=223 (K)	V_y(mV)	-0.61	-0.60	-0.59	-0.58	-0.56	-0.56	-0.55	-0.53	-0.52	-0.51	-0.46	-0.40	-0.36	-0.32
	V_R(mV)	2.27	2.22	2.15	2.01	1.84	1.73	1.56	1.39	1.29	1.11	0.94	0.72	0.61	0.53
	ΔT_x (K)	7.47	7.30	7.07	6.59	6.02	5.60	5.00	4.40	4.06	3.38	2.78	2.05	1.70	1.45
	ΔT_y (K)	-2.07	-2.05	-2.02	-1.99	-1.93	-1.90	-1.87	-1.82	-1.79	-1.73	-1.59	-1.36	-1.22	-1.11
T=273 (K)	V_y(mV)	-0.61	-0.61	-0.59	-0.57	-0.55	-0.54	-0.53	-0.51	-0.50	-0.48	-0.44	-0.37	-0.34	-0.31
	V_R(mV)	2.17	2.12	2.05	1.91	1.76	1.64	1.48	1.32	1.23	1.06	0.88	0.68	0.57	0.51
	ΔT_x (K)	7.02	6.85	6.62	6.15	5.62	5.19	4.66	4.11	3.79	3.15	2.59	1.89	1.57	1.37
	ΔT_y (K)	-2.04	-2.04	-1.98	-1.92	-1.87	-1.81	-1.78	-1.72	-1.69	-1.63	-1.49	-1.25	-1.14	-1.05
T=295 (K)	V_y(mV)	-0.56	-0.56	-0.55	-0.53	-0.51	-0.50	-0.48	-0.47	-0.46	-0.44	-0.39	-0.34	-0.30	-0.28
	V_R(mV)	1.99	1.94	1.88	1.76	1.60	1.50	1.36	1.21	1.13	0.97	0.82	0.63	0.53	0.47
	ΔT_x (K)	6.46	6.25	6.07	5.64	5.13	4.77	4.29	3.77	3.47	2.90	2.38	1.78	1.48	1.27
	ΔT_y (K)	-1.90	-1.87	-1.84	-1.78	-1.72	-1.69	-1.63	-1.57	-1.54	-1.48	-1.33	-1.15	-1.03	-0.94
T=343 (K)	V_y(mV)	-0.60	-0.59	-0.57	-0.56	-0.54	-0.52	-0.50	-0.49	-0.47	-0.45	-0.41	-0.34	-0.31	-0.29
	V_R(mV)	2.05	1.99	1.92	1.79	1.65	1.53	1.38	1.24	1.14	0.98	0.81	0.63	0.53	0.47
	ΔT_x (K)	6.61	6.42	6.22	5.74	5.25	4.84	4.35	3.80	3.51	2.93	2.39	1.77	1.45	1.29
	ΔT_y (K)	-2.03	-2.00	-1.93	-1.87	-1.81	-1.74	-1.68	-1.64	-1.58	-1.52	-1.39	-1.16	-1.03	-0.97
T=373 (K)	V_y(mV)	-0.64	-0.62	-0.60	-0.58	-0.57	-0.55	-0.52	-0.51	-0.50	-0.47	-0.43	-0.43	-0.36	-0.32
	V_R(mV)	2.12	2.07	2.01	1.86	1.71	1.58	1.42	1.28	1.19	1.00	0.84	0.64	0.55	0.49
	ΔT_x (K)	6.77	6.57	6.38	5.89	5.37	4.98	4.43	3.91	3.61	2.99	2.44	1.79	1.46	1.30
	ΔT_y (K)	-2.15	-2.08	-2.02	-1.95	-1.89	-1.82	-1.73	-1.69	-1.66	-1.56	-1.43	-1.43	-1.20	-1.07

BIBLIOGRAPHY

1. R. R. Zarr, "History of Testing Heat Insulators at the National Institute of Standards and Technology," Building and Fire Research Laboratory, National Institute of Standards and Technology , Gaithersburg, MD 20899, (reprinted from ASHRAE Transactions, 2001), Vol. 107, No.2

2. C. J. Dey, A. J. Read, R. E. Collins, M. Brunotte, “A guarded cold plate apparatus for absolute measurement of heat flow,” International Journal of Heat and Mass Transfer, Vol. 41, pp. 3099-3108, (1998)

3. R. P. Tye, L. Kubicar, and N. Lockmuller, “The Development of a Standard for Contact Transient Methods of Measurement of Thermophysical Properties,” International Journal of Thermophysics, Vol. 26, No, 6, (2005).

4. M. Anis-ur-Rehman, and A. Maqsood, "Measurement of Thermal Transport Properties with an Improved Transient Plane Source Technique," International Journal of Thermophysics, Vol. 24, No.3, (2003).

5. H.S. Carslaw, and J.C. Jaeger et al., "Conduction of Heat in Solids," 2nd ed., (Oxford University Press, 1959)

6. W. R. Davis, "Determination of the thermal conductivity of Refractory Insulating Materials by the Hot-Wire Method," American Society for Testing and Materials, pp. 186-199, (1978).

7. O. M. Corbino, "Periodic variation of resistance of metallic filaments on alternating current," Atti della Reale Accademia Nazionale dei Lincei, Vol. 20, pp. 222-228, (1911).

8. N. O. Birge, and S. R. Nagel, "Wide-frequency specific heat spectrometer," Review of Scientific Instruments, Vol. 58, No.8, 1464-1470, (1987).

9. D. G. Cahill, and R. O. Pohl, "thermal conductivity of amorphous solids above the plateau," The American Physical Society, Vol. 35, No. 8, pp. 4067-4073, (1987).

10. G. A. Slack, "Solid State Physics," edited by H. Ehrenreich, F. Seitz, and D. Turnbull, (Academic Press, NY, 1979), Vol. 34, p. 1

11. T.M.Tritt, "Recent trends," (Academic Press, 2000).

12. J. F. Xing, X. J. Kun, L. B. Yang, X. Yu, H. R. Jin, and L. L. Feng "Thermoelectric Performance of Poly(3,4 ethylenedioxythiophene):Poly(styrenesulfonate)," J. CHIN.PHYS.LETT, Vol. 25, No. 6, 2202 (2008).

13. D. D. Koninck, "Thermal Conductivity Measurements Using the 3-Omega Technique: Application to Power Harvesting Microsystems," Master thesis, Department of Mechanical Engineering, McGill University, Montréal, Canada, 2008, MR53445, p. 2-13

14. D. D. Koninck, "Thermal Conductivity Measurements Using the 3-Omega Technique: Application to Power Harvesting Microsystems," Master thesis, Department of Mechanical Engineering, McGill University, Montréal, Canada, 2008, MR53445, p. 2-17

15. K. M. Choi, “Photopatternable Silicon Elastomers with Enhanced Mechanical Properties for High-Fidelity Nanoresolution Soft Lithography,” J. Phys. Chem. B, Vol. 109, pp. 21525-21531, (2005).

16. K. C. CHANG, M. S. JENG, C. C. YANG, Y. W. CHOU, S. K. WU, M. A. THOMAS, and Y. C. PENG, “The Thermoelectric Performance of Poly(3,4-ethylenedioxythiophene)/ Poly(4-styrenesulfonate) Thin Films, “J. ELECTRONIC MATERIALS, Vol. 38, No. 7, (2009).

17. D. G. Cahill, H. E. Fischer, T. Klitsner, E. T. Swartz, and R. O. Pohl, “Thermal conductivity of thin films: Measurements and understanding,” American Vacuum Society, Vol. 7, No. 3, (1989).

18. D. G. Cahill, M. Katiyar, and J. R. Abelson, ”thermal conductivity of a-Si:H thin films,” Physical Rev. B, Vol. 50, No. 9, (1994).

19. R. F. Haglund, Jr. Stephen, L. Johnson, H. K. Park, “Electronic and Optical Properties of Polymer Thin Films Deposited by Resonant Infrared Laser Ablation,” Journal of Laser Micro/Nanoengineering (JLMN), Vol. 2, No. 3, pp. 234-240, (2007).

20. X. J. Hu, A. Jain, K. E. Goodson, “Investigation of the natural convection boundary condition in microfabricated structures,” International Journal of Thermal Sciences, Vol. 47, pp. 820–824, (2008)

21. A. Jacquot, B. Lenoir, and A. Dauscher, “Numerical simulation of the 3v method for measuring the thermal conductivity,” JOURNAL OF APPLIED PHYSICS, Vol. 91, No. 7, pp. 4733-4738, (2002).

22. I. K. Moon, Y. H. Jeong, and S. I. Kwun, "The 3ω technique for measuring dynamic specific heat and thermal conductivity of a liquid or solid," J. American Institute of Physics, Vol. 67, No. 1, (1996)

23. S. M. Lee, “Thermal conductivity measurement of fluids using the 3ω method,” REVIEW OF SCIENTIFIC INSTRUMENTS, Vol. 80, 024901(2009).

24. L. B. Yang, L. C. Cong, L. Shan, X. J. Kun, J. F. Xing, L. Y. Zhen, and Z. Zhuo, "Thermoelectric Performances of Free-Standing Polythiophene and Poly(3-Methylthiophene) Nanofilms," J. CHIN.PHYS.LETT, Vol. 27, No. 5, 057201 (2010).

25. G. Wu, J. Yang, S. Ge, Y. Wang, M. Chen, and Y. Chen, “Thermal conductivity measurement for carbon-nanotube suspensions with 3ω method,” Advanced Materials Research, Vols. 60-61, pp 394-398, (2009).

26. K.T. Wojciechowski, R. Zybala , R. Mania, “Application of DLC layers in 3-omega thermal conductivity method,” J. Achievements in materials and manufacturing engineering, Vol. 27, No. 2, pp. 512-517, (2009).

27. H. G. Walther, T. Kitzing, Z. Bozoki, G. L. Liakhou, and S. Paolonic, "Probing thermal conductivity variations in excimer laser irradiated polyimide foils," J. APPLIED PHYSICS, Vol. 85, No. 11, (1999).

28. http://www.metrictest.com/catalog/brands/keithley/kei_2400.jsp (accessed July 2010).

29. http://hyperphysics.phy-astr.gsu.edu/hbase/tables/thrcn.html (accessed July 2010).

30. http://www.hukseflux.com/thermalScience/thermalConductivity.html (accessed July 2010).

31. http://www.goodfellow.com/E/Silica.html (accessed July 2010).